UNIVERSITY OF
BATH

**University of Bath**

**Alternative formats**
If you require this document in an alternative format, please contact:
openaccess@bath.ac.uk

# Forecasting the long-term deterioration of a cut slope in high-plasticity clay using a numerical model

**Postill, H.**[a]; **Helm, P.R.**[b]; **Dixon, N.**[a]; **Glendinning, S.**[b]; **Smethurst, J.A.**[c]; **Rouainia, M.**[b]; **Briggs, K.M.**[d]; **El-Hamalawi, A.**[a]; **Blake, A.P.**[c]

[a]Loughborough University, UK
[b]Newcastle University, UK
[c]University of Southampton, UK
[d]University of Bath, UK

## Abstract

This paper details development of a numerical modelling approach that has been employed to forecast the long-term performance of a cut slope formed in high plasticity clay. It links hydrological and mechanical behaviour in a coupled saturated and unsaturated model. This is used to investigate the influence of combined dissipation of excavation-generated excess pore water pressures and seasonal weather-driven near-surface cyclic pore water pressures. Deterioration of slope performance is defined in terms of both slope deformations (i.e. service) and factor of safety against shear failure (i.e. safety). Uniquely, the modelling approach has been validated using 16 years of measured pore water pressure data from multiple locations in a London Clay cut slope. Slope deterioration was shown to be a function of both construction-induced pore water pressure dissipation and seasonal weather-driven pore water pressure cycles. These lead to both transient and permanent changes in factor of safety due to effective stress variation and mobilisation of post-peak strength reduction over time, respectively, ultimately causing shallow first-time progressive failure. It is demonstrated that this long-term (90 year) deterioration in slope performance is governed by the hydrological processes in the weathered near surface soil zone that forms following slope excavation.

**Reference:**
Postill, H., Helm, P.R., Dixon, N., Glendinning, S., Smethurst, J.A., Rouainia, M., Briggs, K.M., El-Hamalawi, A., Blake, A.P. (2020). Forecasting the long-term deterioration of a cut slope in high-plasticity clay using a numerical model. *Engineering Geology*. https://doi.org/10.1016/j.enggeo.2020.105912

# Contents

# 1   Introduction

Uncontrolled deformations of cut slopes along transport infrastructure routes cause reduced service performance (Briggs et al., 2019) leading to delays and disruption to the movement of people and goods, ultimately impacting the economy (Power and Abbott, 2019). In the worst case, car accidents and train derailments due to ultimate limit state slope failures lead to safety performance issues that can result in loss of human life (Rail Accident Investigation Branch, 2017). Therefore, understanding the long-term behaviour of cut slopes is important so that asset management approaches can be implemented to maintain performance at an affordable cost (Spink, 2019). This is in turn set in the context of a deterioration curve to demonstrate a reduction in asset performance over time (see for example Thurlby, 2013).

Shear failures within high-plasticity clay cut slopes are primarily driven by two inter-related processes: dissipation of suppressed post-excavation pore water pressures with associated stress relief (Vaughan and Walbancke, 1973), and annual wetting and drying cycles. These cycles, due to the high plasticity of the material, cause shrink-swell cycles and result in the development of accumulated annual displacements. This process is known as seasonal ratcheting (Take, 2003; Take and Bolton, 2004, 2011). Both of these mechanisms can generate stress changes that induce strain-softening behaviour, localised mobilisation of post-peak strength and stress re-distribution within high-plasticity clay cut slopes. This in turn can lead to progressive slope failure (Skempton, 1964; Potts et al., 1997; Leroueil, 2001; Ellis and O'Brien, 2007). The progressive loss of strength as a result of seasonal stress cycles leading to strength deterioration and progressive failure means that high-plasticity clay slopes can remain stable during one wet event but fail a number of years later due to a similar magnitude event (Take and Bolton, 2011; Postill et al., 2020). This study uses numerical modelling to show how deterioration of slope performance, as defined using both slope deformations and factor of safety against shear failure respectively, is driven by a combination of post-excavation pore water pressure dissipation and long-term cycling of weather driven near surface pore pressures that produce reductions in soil strength (Stirling et al., 2017, 2020).

Elia et al. (2017) illustrate the difficulty of modelling soil-vegetation-atmosphere-driven long-term cyclic pore water pressures and highlight the limited data sets available to validate model behaviour. In addition, Elia et al. (2017) discuss the significance of including coupled hydro-mechanical behaviour in order to capture long-term soil strength deterioration due to shrink-swell stress cycles that ultimately lead to progressive failure. To date, numerical simulations of long-term clay slope behaviour have had one or more of the following characteristics; non-softening behaviour that can only analyse transient changes in effective stress (Oh and Lu, 2015; Tsiampousi et al., 2017); use has been made of simple wetting and drying boundary conditions to explore stress cycles; or where progressive failure is considered, this is undertaken within a saturated model (Kovacevic et al., 2001; Nyambayo et al., 2004; O'Brien et al., 2004), which excludes the effects of unsaturated behaviour in the near surface of the slope. Rouainia et al. (2009) demonstrated use of an approach employing daily boundary conditions and a two-phase flow approach to model unsaturated conditions and coupled hydro-mechanical behaviour to investigate soil-vegetation-atmosphere interactions on performance of an infrastructure embankment in high-plasticity clay. Accumulated seasonal rainfall infiltration has also been shown to have an effect on slope stability in a number of modelling studies (Rahardjo et al., 2001; Alonso et al., 2003; Calvello et al., 2008; Zhang et al., 2014; Cotecchia et al., 2019). The importance of near surface behaviour, particularly for the modelling of pore pressures, is

emphasised in Rahardjo et al. (2013). The methodology derived by Rouainia et al. (2009) was later used to investigate the stability of a natural slope in glacial till (Davies et al., 2014) and applied to a cut slope. This cut slope model also began to introduce deterioration into the approach adopted here by demonstrating the reduction in residual factor on the ultimate failure surface over time (Rouainia et al., 2020). The importance of the inclusion of the air phase and the effect on model results is further demonstrated by Cho (2016). Postill et al., 2020, also using a coupled two-phase flow and mechanical formulation, showed that the mechanism of ratcheting due to seasonal pore water pressure cycles, as observed in centrifuge experiments, could be successfully modelled numerically. That work demonstrated the effect of seasonal stress cycles on plastic strain accumulation and progressive failure due to prolonged wetting as well as continued seasonal stress and included a validation of both the pore water pressure cycles and the mechanical response.

A significant further advance is made in the current paper using a two-phase flow numerical procedure (after Postill et al., 2020) to study long-term deterioration of a highway cut slope in high plasticity clay near Newbury, UK. Importantly, it also responds to the review carried out by Elia et al. (2017) by validating the numerical model outputs using a 16-year time series of field measurements from the slope (Smethurst et al., 2012). The primary mechanism of deterioration studied is strain-softening due to the development of plastic shear strains caused by: 1) dissipation of construction induced negative excess water pressures; and 2) annual weather-driven stress cycles causing seasonal ratcheting. The approach allows both the deep-seated saturated processes (i.e. post-excavation pore water pressure dissipation) and near-surface unsaturated processes (i.e. seasonal ratcheting) to be modelled simultaneously. Daily weather boundary conditions were considered, and forecasts of long-term behaviour have been developed using a synthetic weather sequence.

## 2   Newbury cutting case study

The slope investigated in this work is a highways cutting, dating from 1997, formed within the London Clay (Fig. 1). The site has been monitored to investigate changes in soil moisture content, pore water pressures and surface-atmosphere interaction (Smethurst et al., 2006, 2012). In the study area, the London Clay formation extends to a depth of 20 m, with the upper 2.5 to 3.0 m being weathered beneath the original ground profile (Smethurst et al., 2006). The slope is grass covered with occasional shrubs. It is 8 m high and has an angle of 1 in 3.5. Fig. 1 shows the slope geometry, piezometer positions and location of the slope. A detailed description of the field monitoring approach and equipment installed at Newbury, and interpretation of factors controlling near surface response to seasonal weather are presented by Smethurst et al. (2006, 2012).
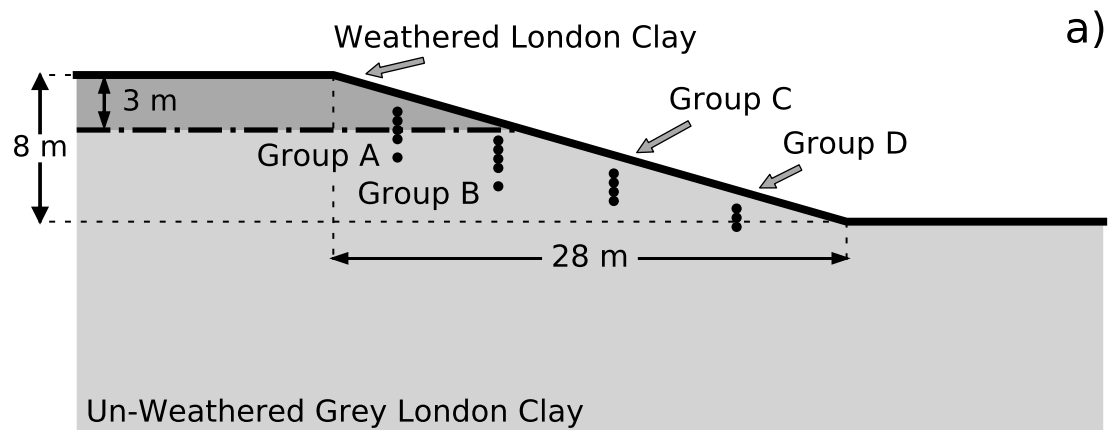
Figure 1: a) geometry of slope and location of monitoring equipment; b) location

# 3    Numerical modelling approach

The numerical analyses reported in this paper used the finite difference software FLAC two-phase flow (FLAC-TP) (Itasca, 2016), which has been modified to include user-specified algorithms described in this section and in Postill et al., 2020. FLAC-TP is formulated for the simulation of wetting and non-wetting fluids flowing within a continuum model, allowing hydro-mechanical coupling. The approach adopted uses a displacement-pore pressure ($u - p$) formulation and assumes the fluids (i.e. water and air) within the soil are homogeneous and idealised (i.e. fluids are immiscible). The software and approach were used and discussed by Postill et al., 2020 for the modelling of the seasonal ratcheting mechanism validated against centrifuge experiments and the London Clay local-strain softening was validated in Rouainia et al. (2020). In brief, inter-particle stresses are described by Bishop's generalised effective stress, $\sigma_B^{'}$, as follows (Bishop, 1959): Eq. (1).

$$\sigma_B^{'} = (\sigma - u_a) + \chi(u_a - u_w) \tag{1}$$

where $\chi$, is the effective stress parameter. In this model, the degree of saturation, $S_w$, is used as an approximation for $\chi$. It has been recognised in the literature that $S_w$ can be used to quantify the Bishop's effective stress parameter $\chi$ at high degrees of saturation, such as those found in the typical range of pore water suctions predicted in this work (Khalili et al., 2004; Nuth and Laloui, 2008).

Hydrogeological behaviour is a function of effective saturation ($S_e$), linked to matric suction ($s$) through unimodal van Genuchten (1980) soil water retention curves (SWRC), Eq. (2).

$$s = \alpha \left[ S_e^{-\frac{1}{m}} - 1 \right]^{1-m} \tag{2}$$

where $\alpha$ and $m$ are fitting parameters.

To account for the reduction in hydraulic conductivity ($K_{sat}$) as the soil becomes unsaturated, relative hydraulic conductivity of the water ($K_r^w$) and air ($K_r^a$) phases are calculated as per Eqs. (3) and (4).

$$K_r^w = K_{sat} \cdot S_e^{0.5} \left[ 1 - \left( 1 - S_e^{\frac{1}{m}} \right)^m \right]^2 \tag{3}$$

$$K_r^a = K_{sat} \frac{\mu_w}{\mu_g} \cdot (1 - S_e)^{0.5} \left[ 1 - S_e^{\frac{1}{m}} \right]^{2m} \tag{4}$$

where $\mu_w$ and $\mu_g$ are the fluid and gas dynamic viscosities, respectively.

In this work, slope performance is defined in terms of factor of safety (FoS) against ultimate limit state failure and is classified as being unacceptable once failure has occurred (FoS<1). The effective stress changes due to dissipation of construction induced pore pressure and seasonal wetting and drying cycles would occur regardless of soil type. However, for progressive failure, which is the critical mechanism driving deterioration of the soil shear strength in high plasticity clays, a strain softening constitutive model is required. The adopted approach could also be applied to lower plasticity materials that undergo similar stress cycles, however the magnitude of strength reduction will be lower due to the increased residual strength in lower plasticity soils.

Analyses using strain-softening models can be compromised by mesh dependency (Bažant and Pijaudier-Cabot, 1988; Vermeer and Brinkgreve, 1994; Di Prisco and Imposimato, 2003; Galavi and Schweiger, 2010). To minimise this in the numerical solution, a nonlocal regularisation technique was adopted, where nonlocal plastic strains ($\varepsilon^{p*}$) are obtained by averaging local plastic strains ($\varepsilon^{ps}$), calculated using the Mohr-Coulomb constitutive model (Summersgill et al., 2017b; Postill et al., 2020). $\varepsilon^{ps}$ in FLAC is derived as per Eq. (5) (Itasca, 2016):

$$\Delta\varepsilon^{ps} = \frac{1}{6}\Big[\,\big(\,2\Delta\varepsilon_1^p - \Delta\varepsilon_3^p\,\big)^2 + \big(\,\Delta\varepsilon_1^p + \Delta\varepsilon_3^p\,\big)^2 + \big(\,2\Delta\varepsilon_3^p - \Delta\varepsilon_1^p\,\big)^2\,\Big]^{\frac{1}{2}} \tag{5}$$

in which $\Delta\varepsilon_j^p, (\,j = 1, 3\,)$ are the principle plastic strain increments.

Plastic strain averaging is calculated using Eq. (6):

$$\varepsilon_m^{p*} = \frac{1}{V_w}\sum_{m=1}^{m_{sp}}\omega_m' \cdot \varepsilon_m^{ps} \cdot V_m \tag{6}$$

where $V_w = \sum_{m=1}^{m_{sp}}\omega_m' \cdot V_m$ = weighted volume. The weighting function ($\omega'$) adopted in this work is that proposed by Galavi and Schweiger (2010). See Eq. (7).

$$\omega'(\,r\,) = \frac{r}{l}e^{-(\frac{r}{l})^2} \tag{7}$$

where $r$ is the distance between the calculation point and the neighbouring stress point and $l$ is the internal length which controls the distance over which neighbouring strains effect the strain calculation. This weighting function was shown to be the least mesh-dependent of a number considered by Summersgill et al. (2017b) for analysis of clay cut slopes.

## 3.1   Material properties

Newbury cutting is formed within London Clay; and strain-softening behaviour from previous modelling studies in this material has informed the parameters adopted in the modelling (Potts et al., 1997; Kovacevic et al., 2007, 2013; Ellis and O'Brien, 2007; Rouainia et al., 2009; Summersgill et al., 2018) as well as laboratory and field data (Bromhead, 1978; Bromhead and Dixon, 1986).

The elastic behaviour makes use of a mean effective stress dependent model, where Young's modulus ($E$) is derived from Bishop's generalised mean effective stress ($\sigma_B'$) as per Eq. (8).

$$E = \frac{E_0(\,\sigma_B' + 100\,)}{100} \geq E_{min} \tag{8}$$

where $E_0$ is the reference Young's modulus at zero mean effective stress and $E_{min}$ is the minimum allowable Young's modulus.

The stiffness model was calibrated against swelling tests undertaken on London Clay samples (Hight et al., 2007) taken at a depth similar to the cutting height modelled in this work (8.9 m). The swelling response from this and other published work on the modelling of excavations in London Clay are also included by way of comparison (Potts et al., 1997; Kovacevic et al., 2007). Fig. 2 shows the ability of FLAC to replicate the swelling behaviour shown in Potts et

al. (1997), however when this is compared to the more recent data of Hight et al. (2007), it tends to overestimate the magnitude of swelling at vertical stresses between approximately 20 and 100 kPa. As such a minimum bulk and shear modulus were specified based on the values adopted by Jurečič et al. (2013). The resulting swelling profile more closely matches the field data.
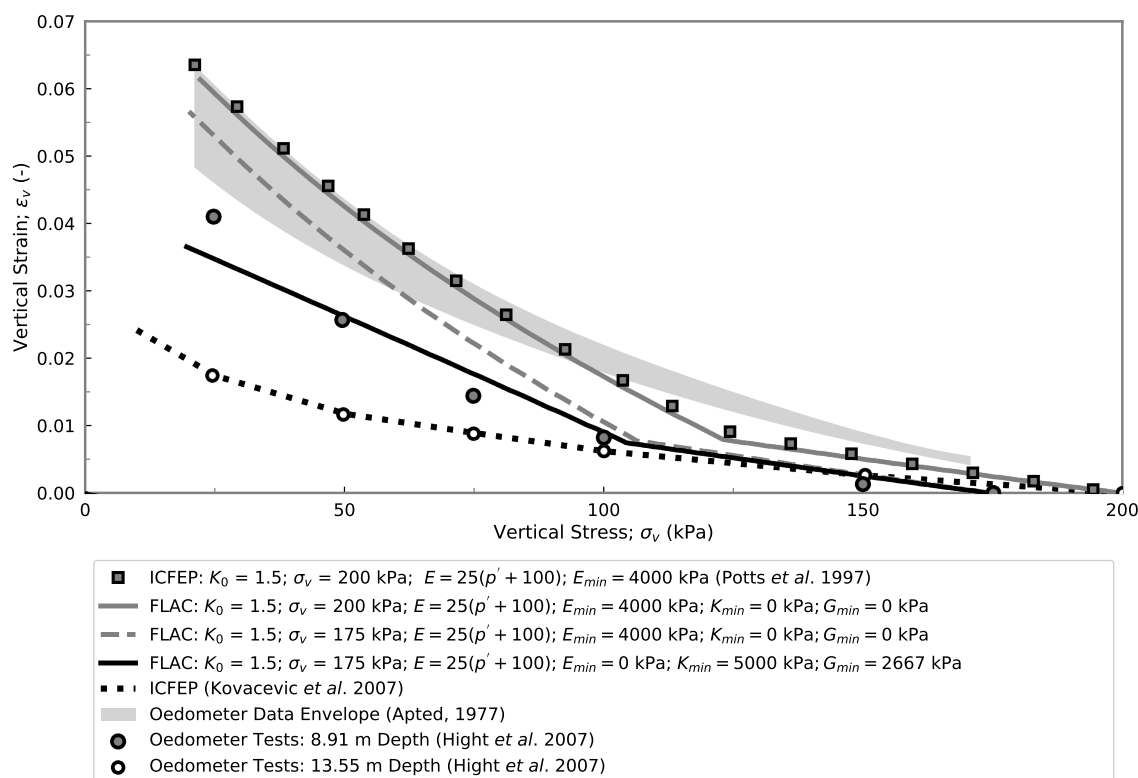


Figure 2: Calibration of the stiffness model against oedometer swelling tests (Apted, 1977; Hight et al., 2007) and comparison with previously adopted stiffness models (Potts et al., 1997; Kovacevic et al., 2007; Rouainia et al., 2020).

Strength is modelled using a Mohr-Coulomb strength envelope that combines internal friction angle ($\phi'$) and apparent cohesion ($c'$). Shear strength/shear strain behaviour is incorporated via definition of peak, post peak and large displacement residual strength properties and the respective strains required for mobilisation.

It should be noted that in this work, the post peak strength adopted is equal to the average strength at failure from the back analysis of slope failures in the field (Bromhead, 1978; Bromhead and Dixon, 1986). This is often described as residual strength by other authors (Potts et al., 1997; Kovacevic et al., 2007; Ellis and O'Brien, 2007; Summersgill et al., 2018).

In this work the adopted residual strength is derived from ring shear testing of London Clay at large displacements (see for example Bishop et al., 1971; Lupini et al., 1981) and includes a total loss of cohesive strength and a further reduction in friction angle as used in Rouainia et al. (2020) where the local strain softening model was also validated for London Clay.

As described in the numerical modelling approach section (see Eqn. 7), the non-local strain softening model adopted here introduces an additional parameter (the internal length; $l$) that

influences the softening rate once plastic strains occur. As such it was necessary to calibrate the model to ensure the adopted softening criteria were appropriate to the adopted mesh (as the non-local model will reduce, but not eliminate, mesh dependency).

The calibration was based on the methodology summarised in Summersgill et al. (2017b) where a series of biaxial tests were simulated on models with differing mesh density. The results of these models are summarised in Fig. 3. The accepted local strain softening rate for London Clay in a model with 1 m elements (Summersgill et al., 2017b) is used as the reference or target softening rate for the non-local softening model. It can be seen that in the local softening models, the mesh size has a large effect on the softening rate with the rate decreasing as mesh size increases. The non-local approach reduces, but does not eliminate, the mesh dependency of the model results especially in coupled hydro-mechanical models. The non-local results, for elements of 0.5 and 0.75 m, bracket the accepted local softening rate, with the 0.5 m model being more conservative. As such, 0.5 m elements were adopted in this work.
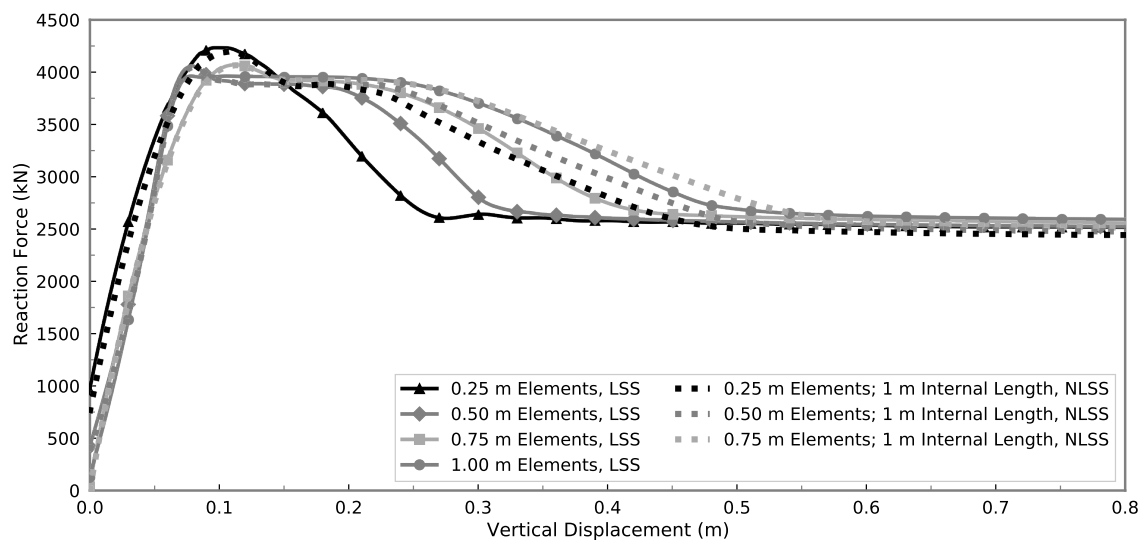


Figure 3: Results of numerically modelled biaxial tests on meshes with different densities and using local (LSS) and non-local strain softening (NLSS) to allow calibration of the softening model.

To avoid excessive and unrealistic surface deformations where the effective shear strength may reach very low values at large residual strains, the post peak average field failure strength is adopted as the residual strength in the upper 1 m. The parameters used are summarised within Table 1 and shown graphically in Fig. 4.
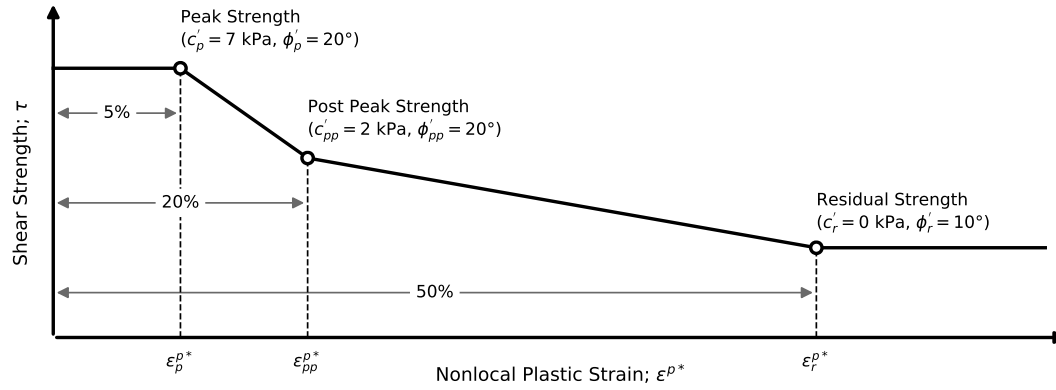
Figure 4: London Clay strain-softening model behaviour.

Table 1: Mechanical material properties (Potts et al., 1997; Kovacevic et al., 2007, 2013; Ellis and O'Brien, 2007; Rouainia et al., 2009, 2020; Jurečič et al., 2013; Summersgill et al., 2017a, 2018).

| **London Clay strain-softening properties** | |
| --- | --- |
| Peak nonlocal plastic strain | 5% |
| Post peak nonlocal plastic strain | 20% |
| Residual nonlocal plastic strain | 50% |
| Internal length (m) | 1.0 |
| Peak cohesion (kPa) | 7.0 |
| Post peak cohesion (kPa) | 2.0 |
| Residual cohesion (kPa) | 0.0[#] |
| Peak friction angle (°) | 21.0 |
| Post peak friction angle (°) | 13.0 |
| Residual friction angle (°) | 10.0[#] |
| Dilation angle (°) | 0.0 |
| **London Clay stiffness properties** | |
| Young's modulus, $E$ (kPa) | $2500( \sigma'_B + 100 )/100$[*] |
| Poisson's ratio, $\nu'$ | 0.2 |
| Bulk modulus, $K$ (kPa) | $E/3( 1 - 2\nu )$ |
| $K_{min}$ (kPa) | 5000.0 |
| Shear modulus, $G$ (kPa) | $E/2( 1 + \nu )$ |
| $G_{min}$ (kPa) | 2667.0 |
| **Other** | |
| Bulk density, $\gamma$ (kN/m$^3$) | 20.0 |
| Porosity, $\theta_s$ | 0.45 |
| Coefficient of earth pressure at rest, $K_0$ | 1.5 |

[*]$\sigma'_B$ = Bishop's generalised effective stress (kPa)

[#]Post peak strength adopted in upper 1 m

The presence of vegetation cover on the slope influences soil strength in two ways. The first effect is hydrological, due to the suctions generated by the uptake of water by plant roots, which causes changes in the effective stress, and therefore, soil strength. This is accounted for in the analysis by including potential evapotranspiration in the surface soil water balance model, described in the boundary condition section.

The second effect is due to the direct influence of roots on the mechanical strength of the soil. Whilst it is known root reinforcement has an influence on near-surface soil strength, there is not an accepted consensus in the literature on how this can best be implemented in numerical models (Cohen et al., 2009). Where parameters are suggested (for example as an increase in cohesion) the potential range of values is large and can therefore be the dominating factor that has significant impacts on slope response. Therefore, the mechanical component of soil shear strength enhancement due to vegetation has been omitted from the simulations. As such the modelling results can be considered conservative.

The hydrogeological properties used to represent Newbury cutting are shown in Fig. 5a-c and summarised in Table 2. Dixon et al. (2019) used field measurements to show that a region of increased near-surface saturated hydraulic conductivity had developed within 20 years of the original formation of Newbury cutting. This region has been included in the analysis, see Fig. 5b. Soil water retention properties are void ratio-dependent (Hu et al., 2013) and void ratio increases as a soil weathers as a result of desiccation cracking.

Recent work by Stirling et al. (2017, 2020) also demonstrates the changes in SWRC due to weather-induced soil deterioration in both the laboratory and field. To reflect this, an intact and a weathered London Clay SWRC were adopted in the analysis, see Fig. 5c. The SWRCs used for intact and weathered London Clay were adopted from Briggs et al. (2013) and Croney (1977). The region over which the near-surface saturated hydraulic conductivity and weathered soil water retention properties are applied in the slope model are shown schematically within Fig. 6.

In the numerical model, prior to excavation, the saturated hydraulic conductivity is set to the profile shown in Fig. 5a with the reference datum being the original ground level. The adopted profile is informed by laboratory and field permeability data for the London Clay (Garga, 1970; Dixon and Bromhead, 1999; Dixon et al., 2019). Once excavation was complete, the increased saturated hydraulic conductivity profile is added to the near-surface of the model with a revised datum representing the excavated ground surface.
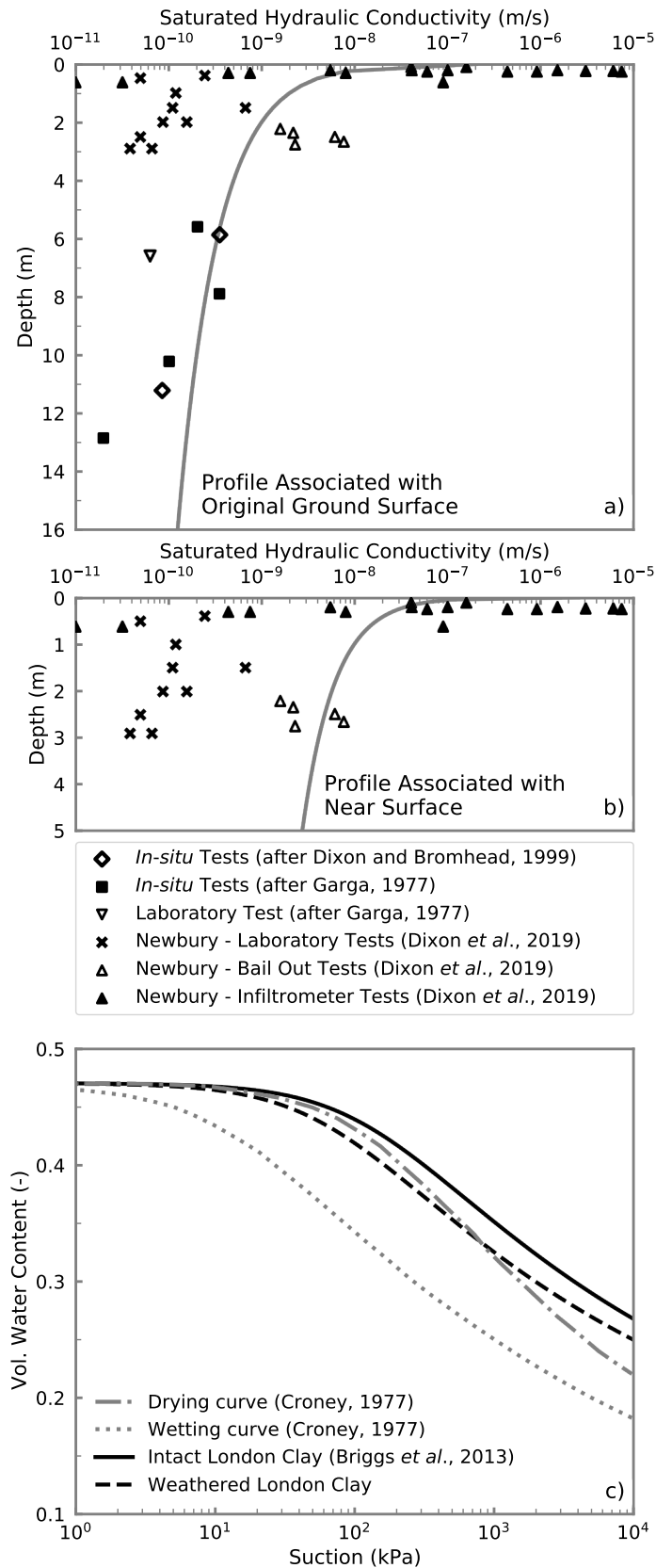
Figure 5: Hydrogeological material properties; a) depth dependent saturated hydraulic conductivity profile associated with original ground surface; b) depth dependent saturated hydraulic conductivity profile associated with near-surface; c) soil water retention properties (after Briggs et al., 2013).

Table 2: Hydrogeological material properties (after Briggs et al., 2013).

| Intact London Clay soil water retention properties | |
|---|---|
| van Genuchten, $\alpha$ (kPa) | 125.0 |
| van Genuchten, $m$ | 0.153 |
| Residual saturation, $S_r^w$ | 0.222 |
| **Weathered London Clay soil water retention properties** | |
| van Genuchten, $\alpha$ (kPa) | 62.5 |
| van Genuchten, $m$ | 0.153 |
| Residual saturation, $S_r^w$ | 0.222 |
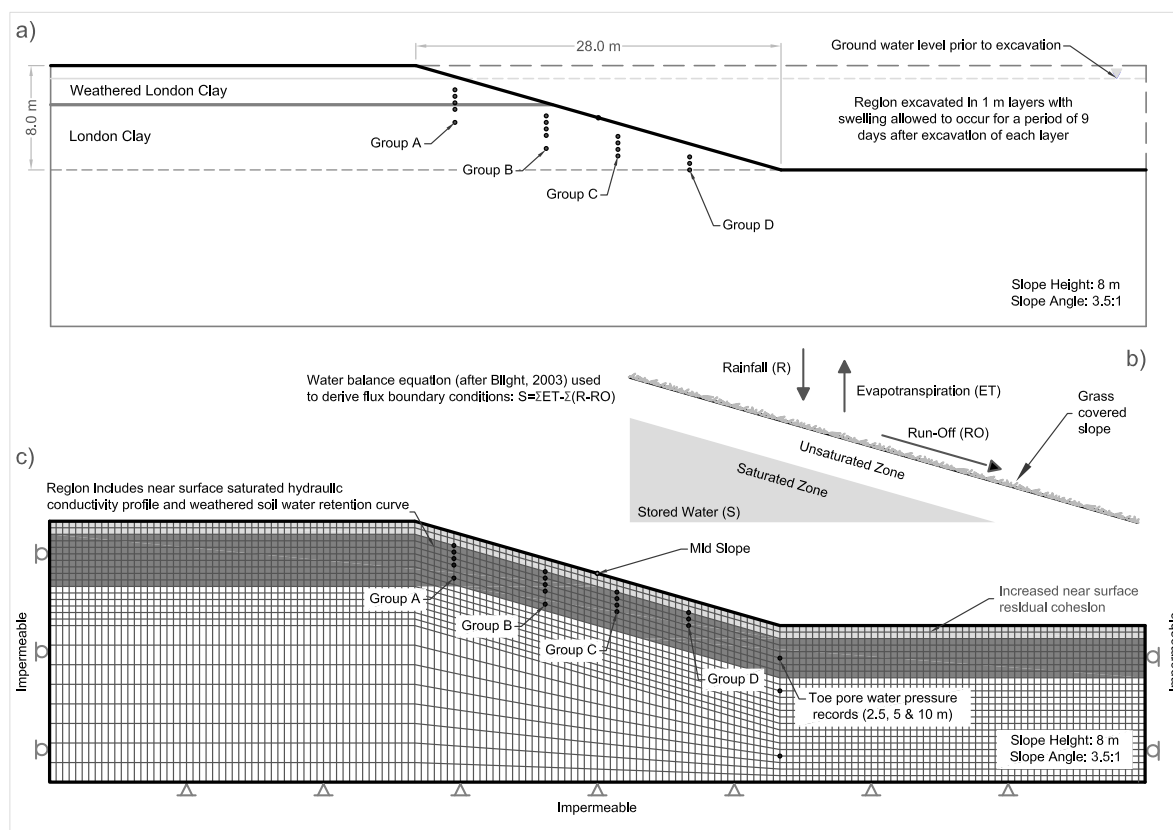


Figure 6: Numerical model configuration (a), schematic boundary conditions (b) and model mesh with monitored history points (c).

The model employed accounts directly, and continuously, for hydraulic conductivity change due to desaturation; but does not incorporate time-dependent changes due to the development of desiccation cracking (Anderson et al., 1982) or the process of progressive SWRC and saturated hydraulic conductivity change resulting from material deterioration mechanisms (i.e. weathering). There is currently little information in the literature on how soil parameters evolve in a developing weathered zone, and so deriving and validating a hydraulic deterioration model that could be employed in the analysis would not be possible at present. However, the effects of these processes were included by assuming they had occurred by the end of excavation (i.e. the newly excavated slope has a fully developed weathered near-surface zone). While there are simplifications in the modelling regarding these complex processes, the work presented advances the current state of modelling long-term behaviour through the inclusion of unsat-

urated behaviour, deteriorated near-surface hydrogeological properties and validation against long time series monitored data.

## 3.2   Initial conditions and cutting excavation

In-situ stresses were initialised assuming a coefficient of earth pressure at rest of $K_0 = 1.5$, and a phreatic surface 1 m below the pre-excavation model ground surface (see Fig. 6a). This in-situ stress is equal to the values used for prior modelling of natural London Clay (Potts et al., 1997; Tsiampousi et al., 2017; Rouainia et al., 2020) and from available in-situ measurements (Hight et al., 2007). The adopted $K_0$ value best captures the swelling response measured by Hight et al. (2007). See Fig. 7.
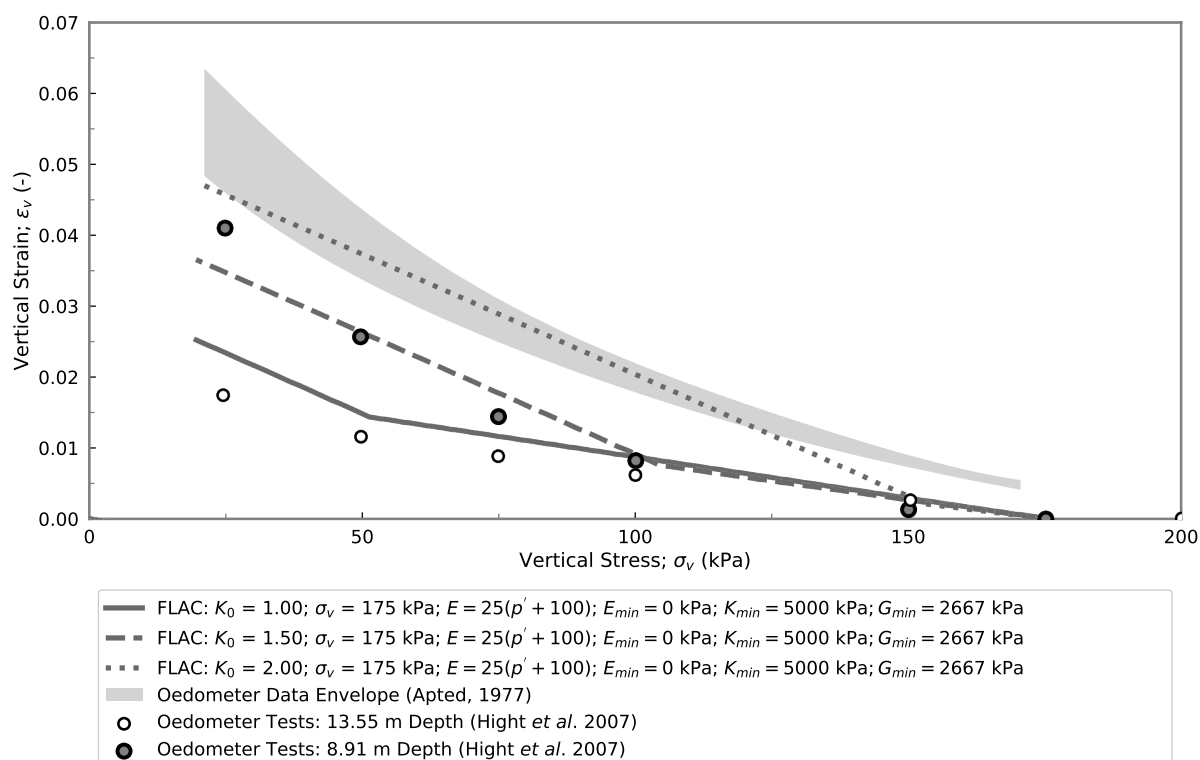


Figure 7: Effect of adopted $K_0$ value on modelled swelling response.

The initial groundwater table is set equal to the UK winter average at 1 m below the surface (Vaughan, 1994) matching that adopted in previous numerical modelling work (Potts et al., 1997; Rouainia et al., 2020). These stresses were then used to derive the initial bulk and shear stiffness distributions ($E_0 = 5000$ kPa) as per Kovacevic et al. (2013). The cut slope excavation was modelled in eight 1 m increments with swelling allowed to occur between each layer for a period of 9 days (region excavated is shown in Fig. 6a). The total excavation time was 72 days, the same excavation rate as modelled for a cut slope in London Clay by Potts et al. (1997). During the post excavation swelling phase and during weather driven cycling of pore water pressures, the stiffness distributions varied using the relationships presented in Table 1.

## 3.3    Boundary conditions

The lateral boundaries were fixed to prevent horizontal movements, and the base was fixed to prevent both horizontal and vertical displacements. The lateral and horizontal boundaries were made impermeable. Surface boundary conditions were applied as daily discharges, obtained through a soil water balance calculation (Blight, 2003) utilising the weather data obtained during monitoring at Newbury cutting (Smethurst et al., 2012), with regional weather data used to infill missing data (i.e. prior to the start of monitoring in 2003). The water balance calculation is shown conceptually within Fig. 6b and given by Eq. (9):

$$SMD = \sum ET - \sum ( R - RO ) \tag{9}$$

where $SMD$ is the soil moisture deficit, $ET$ is actual evapotranspiration (see Eq. 13), $R$ is rainfall and $RO$ is runoff.

From observations, Smethurst et al. (2012) showed run-off occurred only when the soil was at, or very close, to field capacity (i.e. $SMD = 0$ mm). Therefore, within the water balance calculation, run-off was assumed to be zero until the soil was at field capacity.

In order to calculate a daily flux boundary condition, $q_f$ (m/s), the daily change in the soil water balance was calculated. This flux was applied to the numerical analysis and solved for a one-day time increment, the discharge value updated for the next day and the model solved for another day, and so on. Daily flux increments were calculated as shown in Eq. (10).

$$q_f = \frac{\Delta ET - \Delta ( R - RO )}{1000 \times 86400} \tag{10}$$

When the model surface became fully saturated, the surface boundary condition was switched from a discharge boundary to a fixed pore water pressure of 0 kPa until a boundary condition removing water was applied

This is a similar approach to that implemented by Smith (2003). This algorithm was applied to each surface node individually so that a mix of surface pore water pressure fixity and/or discharge could occur at a given time increment depending on the local degree of saturation/available water storage.

### 3.3.1    Past weather data

For the period 2003 to 2019, data from the on-site weather station for Newbury cutting was used. This included rainfall, run-off, and reference potential evapotranspiration ($PET$) calculated using the FAO Penman-Monteith equation (Allen et al., 1998). See Equation. (11).

$$PET = \frac{0.408D( R_n + S_{hf} ) + \gamma \frac{900}{T+273} u_2( e_s - e_a )}{D + \gamma( 1 + 0.34u_2 )} \tag{11}$$

where $D$ is the slope of the vapour pressure curve, $R_n$ is the net solar radiation, $S_{hf}$ is the surface heat flux, $\gamma$ is the psychrometric constant, $T$ is the air temperature, $e_s$ and $e_a$ are the saturation and actual vapour pressures and $u_2$ is the wind speed at 2 m height.

To infill gaps in the weather time series, regional weather data and the Blaney and Criddle (1950) method to derive reference potential evapotranspiration was used. The sources of regional weather data are summarised in Table 3 and the areas of coverage are shown in Fig. 8. Allen et al. (1998) recommend the Blaney and Criddle (1950) method for calculation of potential evapotranspiration where there is a paucity of historical weather data available. The calculation method is shown in Eq. (12) with site-specific calibration factors summarised in Table 4.

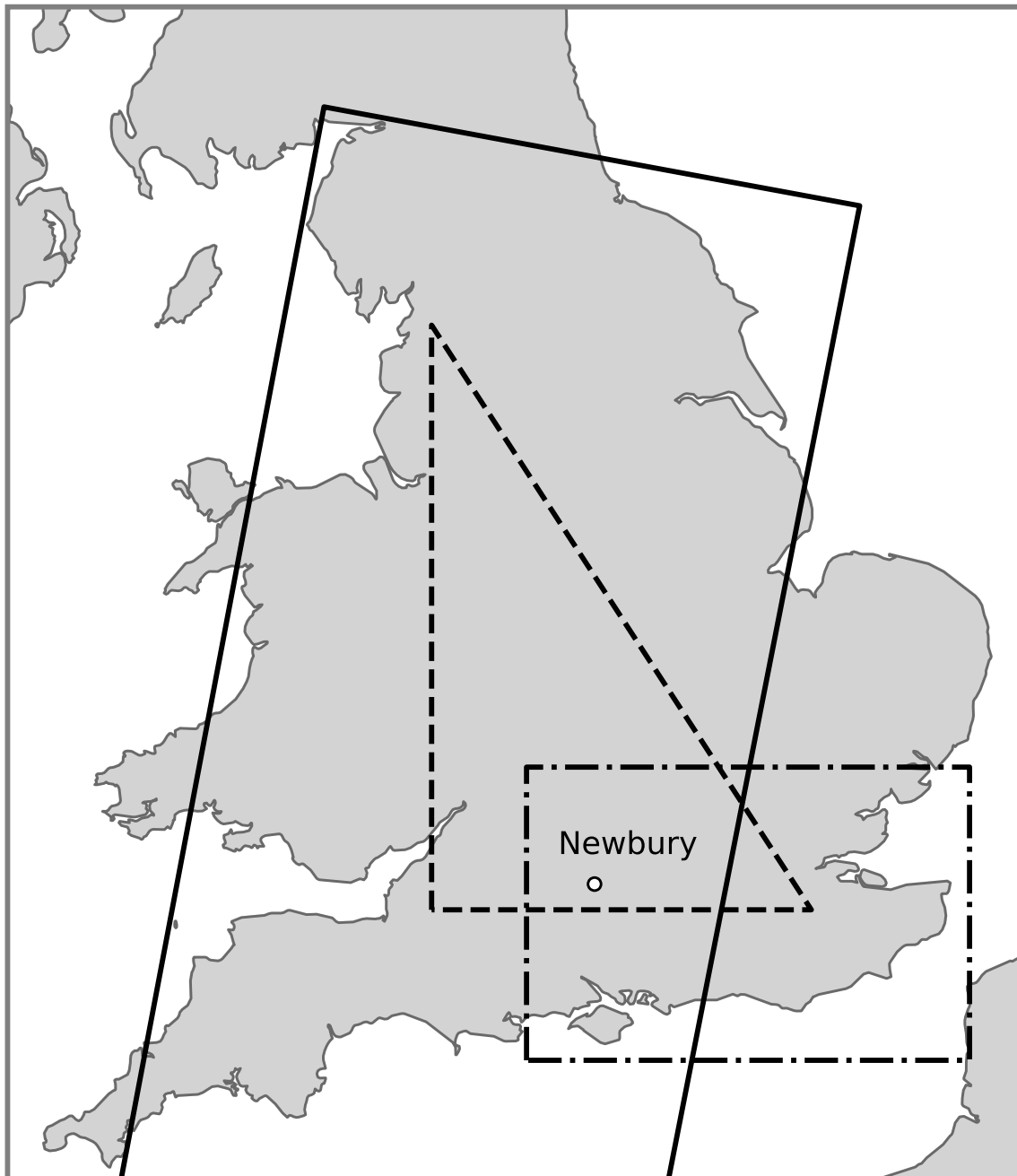$$PET = a + b[\,p(\,0.46T + 8.13\,)\,] \tag{12}$$

where, $a = 0.0043 \cdot RH_{min} - \frac{n}{N} - 1.41$ is a calibration factor in which $RH_{min}$ is the minimum daily relative humidity, $n$ is the actual daily sunshine duration and $N$ is the maximum potential daily sunshine duration.

Table 3: Regional weather data sources.

| Dataset | Name | Variable | Frequency | Time Series | Reference |
|---------|------|----------|-----------|-------------|-----------|
| HadUKP | England and Wales Precipitation (South East England) | Rainfall | Daily | 1931 - Present | (Alexander & Jones, 2000) |
| HadCET | Central England Temperature Record | Mean Temp. | Daily | 1772 - Present | (Parker et al., 1992) |
| HadISDH | Gridded Land Surface Humidity | Relative Humidity | Monthly | 1973 - Present | (Willett et al., 2014) |

Table 4: Site-specific calibration factors for Blaney and Criddle (1950) PET calculation (after Doorenbos and Pruitt, 1977).

| | Parameter | | |
|---------|------|--------|------|
| Month | $p$ | $a$ | $b$ |
| January | 0.19 | -1.059 | 0.52 |
| February | 0.22 | -1.098 | 0.52 |
| March | 0.27 | -1.129 | 0.64 |
| April | 0.31 | -1.151 | 0.64 |
| May | 0.35 | -1.150 | 0.64 |
| June | 0.37 | -1.129 | 0.64 |
| July | 0.36 | -1.141 | 0.64 |
| August | 0.33 | -1.151 | 0.64 |
| September | 0.28 | -1.120 | 0.64 |
| October | 0.24 | -1.076 | 0.52 |
| November | 0.20 | -1.050 | 0.52 |
| December | 0.17 | -1.059 | 0.52 |

Coastline and Land Surface Polygons © Natural Earth. License: Public Domain.

—— HadISDH: Gridded Land Surface Humidity (Willett et al., 2014)

– – – HadCET: Central England Temperature (Parker et al., 1992)

– · – HadUKP: England and Wales Precipitation (Alexander & Jones, 2000)

Figure 8: Regional weather data coverage.

To convert reference potential evapotranspiration into actual evapotranspiration for the soil water balance calculation, the effect of vegetation (using a crop factor, $k_c = 1$ for grass) and soil water retention behaviour were accounted for using the method outlined by Smethurst et al. (2006). This takes into account the readily available and total available water ($RAW$ and $TAW$) in the soil as a function of the stress and wilting points of the vegetation in relation to the soil water retention properties. As suggested by Smethurst et al. (2006), $TAW = 144$ mm and $RAW = 58$ mm. Using this data, actual evapotranspiration ($\Delta ET$) can be calculated in line with Eq. (13) (Clarke et al., 1998; Smethurst et al., 2006).

$$\Delta ET = \begin{cases} \Delta PET \times k_c & \text{for } 0 \leq SMD \leq RAW \\ \Delta PET \times k_c \times \frac{TAW - SMD}{TAW - RAW} & \text{for } SMD > RAW \end{cases} \tag{13}$$

A comparison of annual cumulative rainfall and potential evapotranspiration for regional and site-specific weather data are presented in Fig. 9a and b, with the derived $SMD$ profile shown in Fig. 9c. Fig. 9 shows that regional and site specific weather is comparable and for this exercise is adequate to model the history of the slope and make an assessment of the current condition of Newbury cutting. The boundary conditions for the analysis were generated from the $SMD$ as described in Eq. (9).
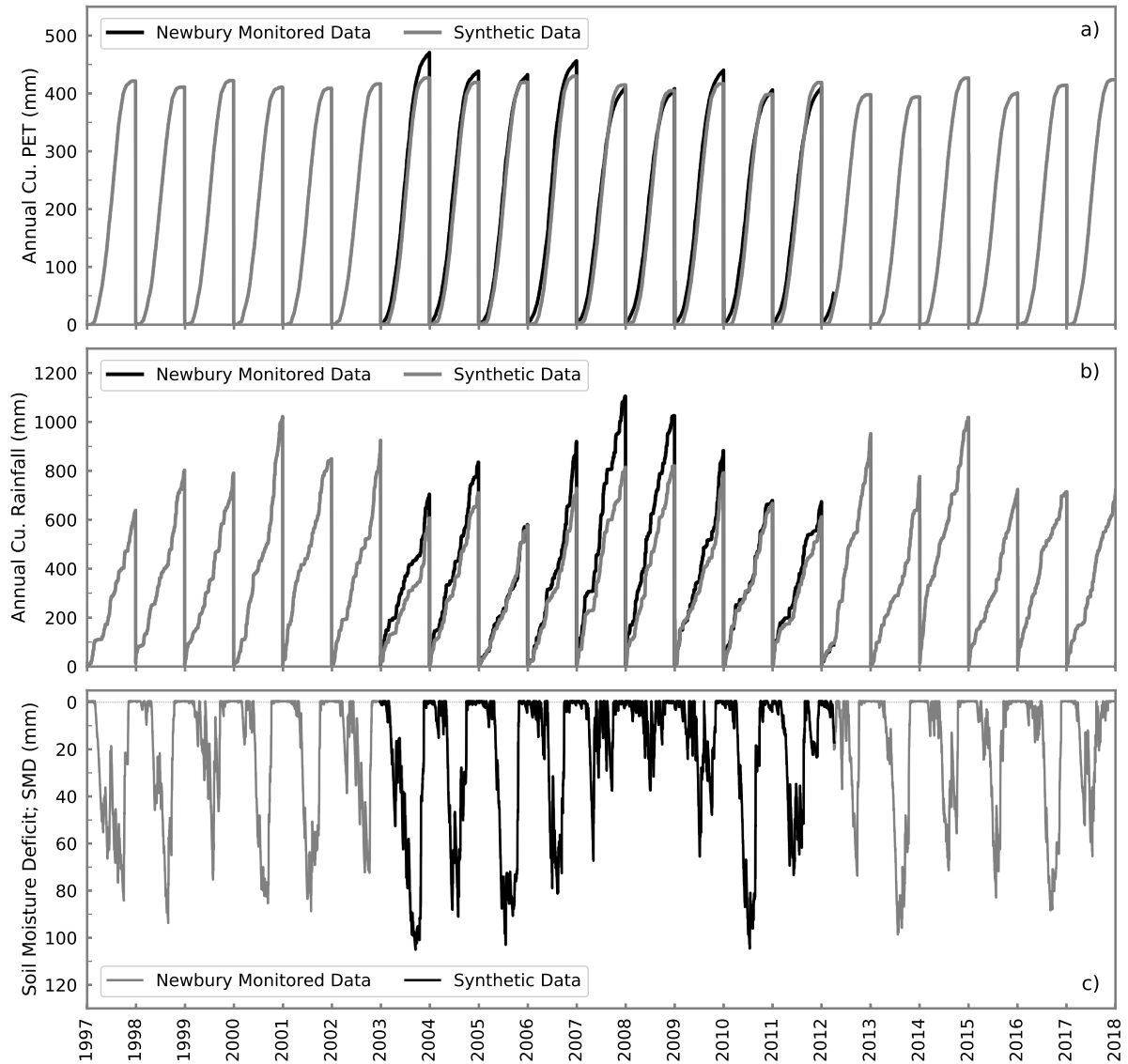
Figure 9: Site-specific (Smethurst et al., 2012) and regional weather data for Newbury cutting; a) cumulative annual rainfall; b) cumulative annual potential evapotranspiration; c) soil moisture deficit used to obtain boundary conditions from construction to 2018.

### 3.3.2   Future weather data

To forecast future performance of Newbury cutting and gain an understanding of long-term behaviour, a future weather sequence was required. Stochastic synthetic daily meteorological data was generated using past seasonal variation in weather patterns using the statistical down-scaling approach described by Wilby et al. (2014).

Baseline regional weather (see Table 3) for the period 1961 to 1990 (see Fig. 10) was used to calibrate the synthetic weather generated. Baseline weather was used to obtain monthly data with cumulative probability distributions created to establish the range and probability of occurrence of temperature and precipitation on any given day of a month. The probability of wet days in each month was also obtained for the baseline period.
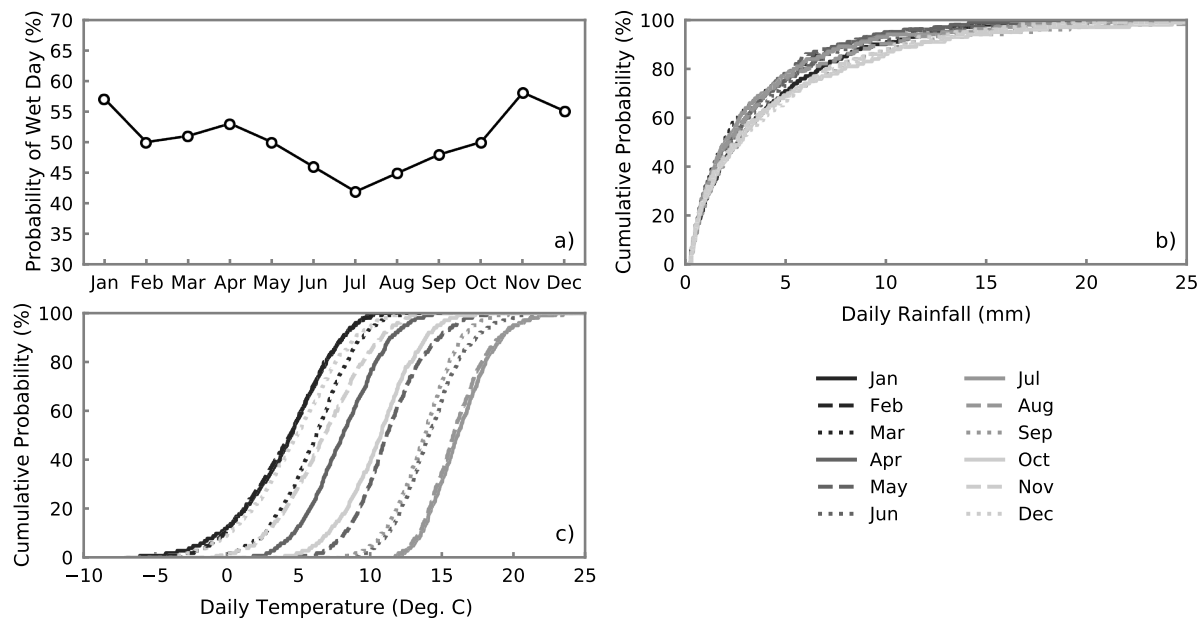


Figure 10: Baseline weather data (1961 to 1990) (temperature data after Parker et al., 1992; rainfall data after Alexander and Jones, 2000); a) probability of a wet day; b) cumulative probability distribution function for daily rainfall; c) cumulative probability distribution function for daily temperature.

The synthetic weather data was then used with the Blaney and Criddle (1950) method and the steps described previously to obtain the SMD and boundary conditions for the analysis. Fig. 11 shows the $SMD$ for the past and future synthetic weather sequence, where the seasonal cycles of $SMD$ for the future synthetic weather are comparable to the past weather.

# 4   Results of modelling Newbury cutting

The following section presents the results of the numerical analysis of Newbury cutting using the methodology, material properties and boundary conditions described. Initially, the period covering the field monitored data is considered (2003 to 2019), then the forecast longer-term behaviour of Newbury cutting is presented. The model geometry and mesh used for the analysis is shown in Fig. 6 along with the locations of the field-monitored and modelled pore water pressures.
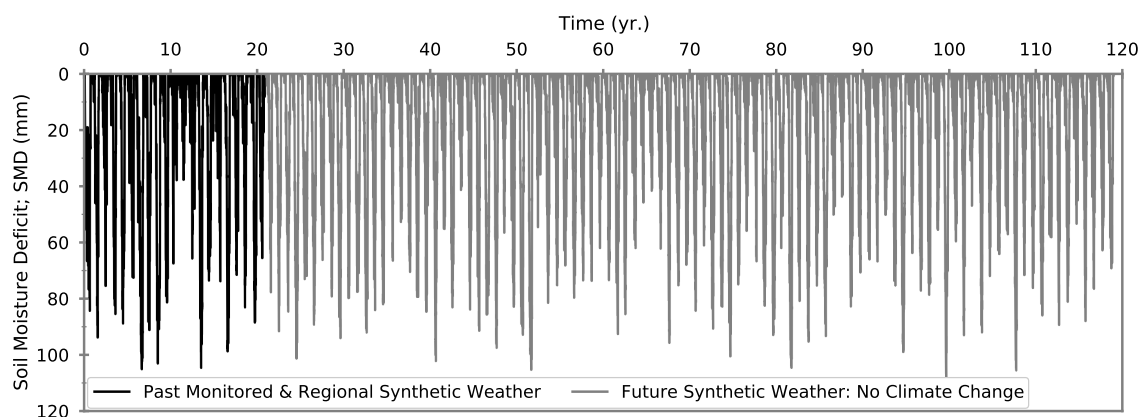
Figure 11: Soil moisture deficit for synthetic future weather sequence.

## 4.1  Hydrogeological response

For the period in which pore water pressure records are available, the near-surface hydrogeo-logical behaviour of the numerical analysis and monitored data were compared for an exemplar location with the results presented in Fig. 12. Where available, tensiometer data is also included for the near surface monitoring points to better indicate the magnitude of near surface suctions. This subset of results from the broader dataset shows that the magnitude and timing of the simulated pore water pressures were representative of the in-situ measurements for different locations and depths across the slope at Newbury cutting. Significantly, prolonged wet periods where suctions were largely dissipated and dry events where large suctions developed were replicated successfully. Comparable fits between modelled and measured pore water pressures were achieved for all the measurement locations shown in Fig. 6.

In addition to comparing modelled and monitored pore water pressures across the slope, pore water pressures below the toe of the slope were considered specifically in order to demonstrate the capabilities of the model to capture post-excavation dissipation of excess pore water pressures. This is shown in Fig. 13 for points 2.5 m, 5.0 m and 10.0 m below the slope toe (for modelled monitoring locations see Fig. 6c).

Fig. 13 shows suppressed pore water pressures due to undrained unloading from excavation. Seasonal cycles of pore water pressures are imposed on these suppressed pore water pressures with a general trend (shown by the fitted lines) of excess pore water pressure dissipation in response to the new boundary conditions. Within the analysis, post-excavation pore water pressure dissipation appears to be complete within 15 to 20 years of construction in the near-surface (i.e. 2.5 m). However, pore water pressure dissipation towards steady state is still occurring at depth (i.e. 5.0 m and 10.0 m) 40 to 50 years post-excavation. This is broadly consistent with the times described in Chandler and Skempton (1974) for London Clay cut slopes. Fig. 13 shows the inter-related nature of long-term behaviour and annual cycles of wetting and drying. Extreme wet and dry periods can be seen to both cause transient fluctuations in pore water pressures and affect the rate of long-term dissipation. However, the overall trend is a dissipation of post-excavation suppressed pore water pressures, which was captured by the numerical model.
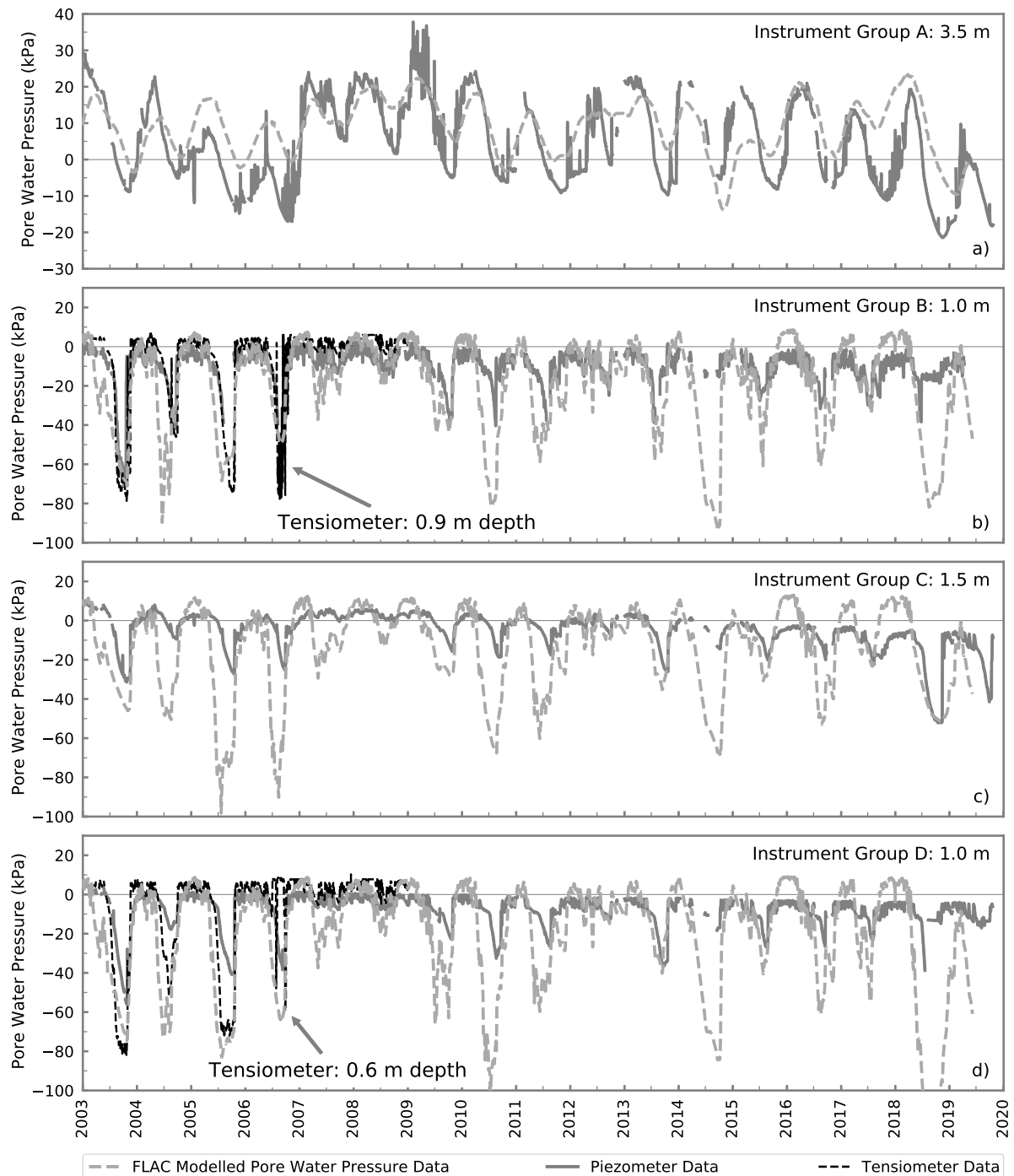
Figure 12: Comparison of hydrogeological response of numerical model and field monitored data for differing piezometers (after Smethurst et al., 2012); a) Group A 3.5 m; b) Group B 1.0 m; c) Group C 1.5 m; d) Group D 1.0 m. Tensiometers at depths indicated.
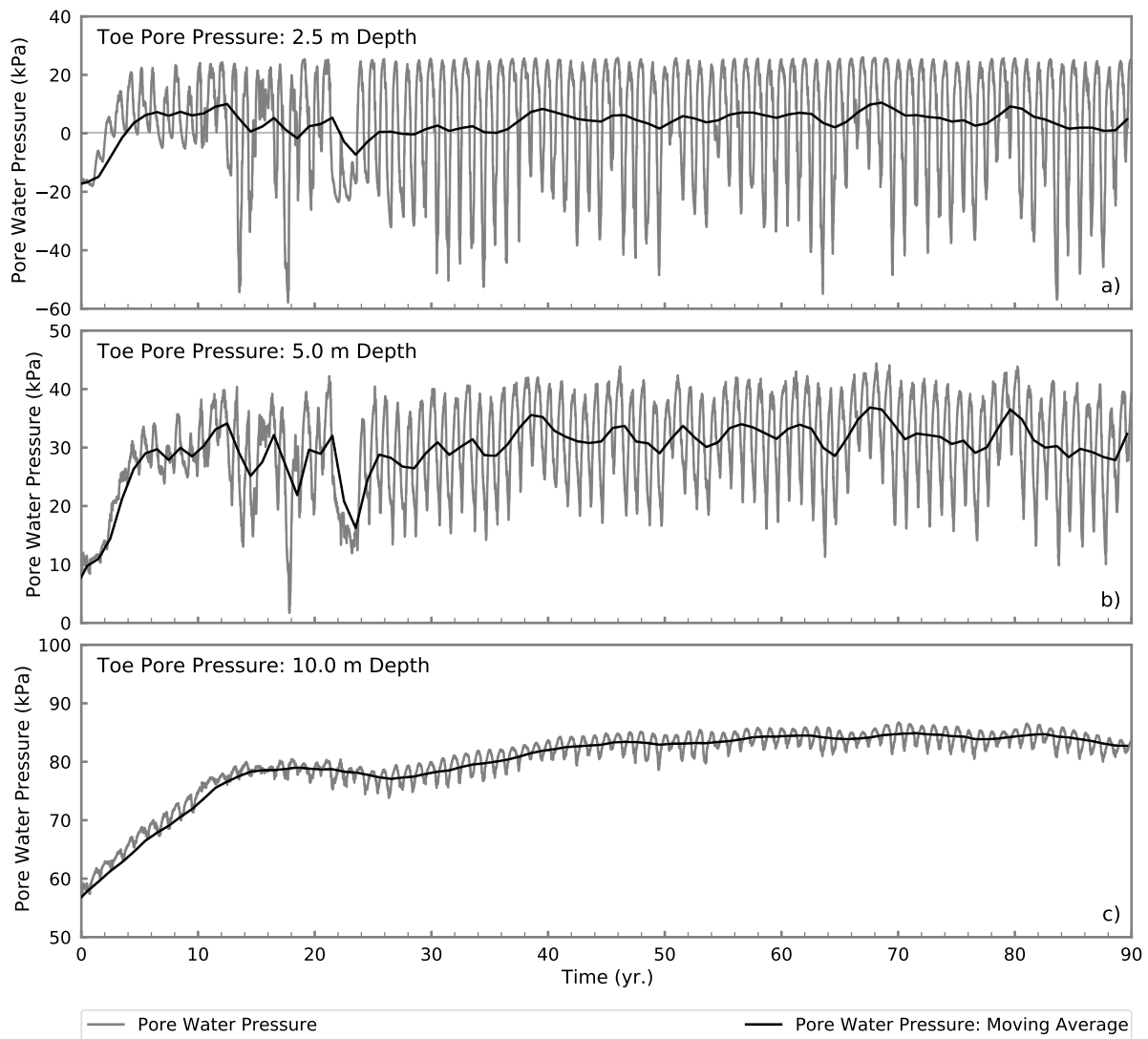
Figure 13: Pore water pressure response post-excavation below toe of slope; a) 2.5 m below toe; b) 5.0 m below toe; c) 10 m below toe.

## 4.2   Mechanical response

The modelled mechanical behaviour as a response to the seasonal pore water pressure cycles and post-excavation dissipation of excess pore water pressures from construction to the end of 2019 is plotted in Fig. 14. Fig. 14a illustrates the modelled pore water pressure record at piezometer D at 1.0 m depth, with mid-slope ground surface displacements shown in Fig. 14b and toe surface displacements in Fig. 14c. For the time period plotted, seasonal shrink-swell displacements give a net upwards and outwards swelling of the slope at the toe and at mid-slope. This initial swelling can be associated with post-excavation pore water pressure dissipation and stress relief, the majority of which at these shallow depths occurs in the first 5 to 7 years (see Figs. 13a and 14a).

To date, in the toe the modelled seasonal movements are dominated by shrink-swell behaviour. Seasonal ratcheting (i.e. outward and downward movement) does not occur at the toe within this time period, however this has started to occur at the mid slope. This is demonstrated in Fig. 14b with a negative net vertical displacement at mid-slope versus Fig. 14c with positive net vertical displacement at the toe during the period in question. This is largely a function of the non-uniform effective stress change and generation of negative pore pressures during excavation which suppress pore pressures to a decreasing extent with increasing distance up the slope and in turn result in differing rates and magnitudes of pore pressure recovery.

Fig. 14a shows that for the time periods, 2007 to 2009, pore water pressures remain close to hydrostatic with only small suctions developing and for 2015 to 2018 the elevated winter pore pressures are sustained for longer than average with relatively low summer suctions, attributable to particularly wet summers (e.g. the summer of 2007 was a 1 in 39 wet event; Smethurst et al., 2012). See Fig. 9b & c. The resultant stress cycles cause a change in the mechanical slope behaviour where the prolonged wetting results in significant swelling displacements (primarily in the horizontal direction) relative to the other seasonal cycles in both the toe and the mid-slope (Fig. 14b & c).

# 5   Forecast of long-term behaviour

The following section presents the results of the numerical model of Newbury cutting when subjected to an additional 90 years of synthetic weather with no climate change effects included, obtained using the method discussed in the boundary condition section (3.3). In order to allow a baseline for comparison and to demonstrate the effect of strain softening on deterioration and differentiate it from the effect of pore pressure change, a control model was run using a perfectly plastic Mohr-Coulomb model without any post peak softening behaviour along with the softening model which was outlined in section 3.1.

In order to quantify deterioration of the slope, a factor of safety (FoS) against ultimate limit state shear failure was calculated for each year of the analysis when the pore water pressures 1.0 m below the toe of the slope reached 0 kPa. This criterion, rather than a fixed point in time each year was selected to reduce the effect of transient pore water pressures leading to associated high levels of variability in the FoS calculations. The specific method for deriving factor of safety is as follows: the algorithm identifies that the pore pressure in the slope toe has exceeded the criterion specified. At this point a temporary save file is created and the coupled fluid mechanical stepping through time is halted. The Mohr-Coulomb constitutive model is then
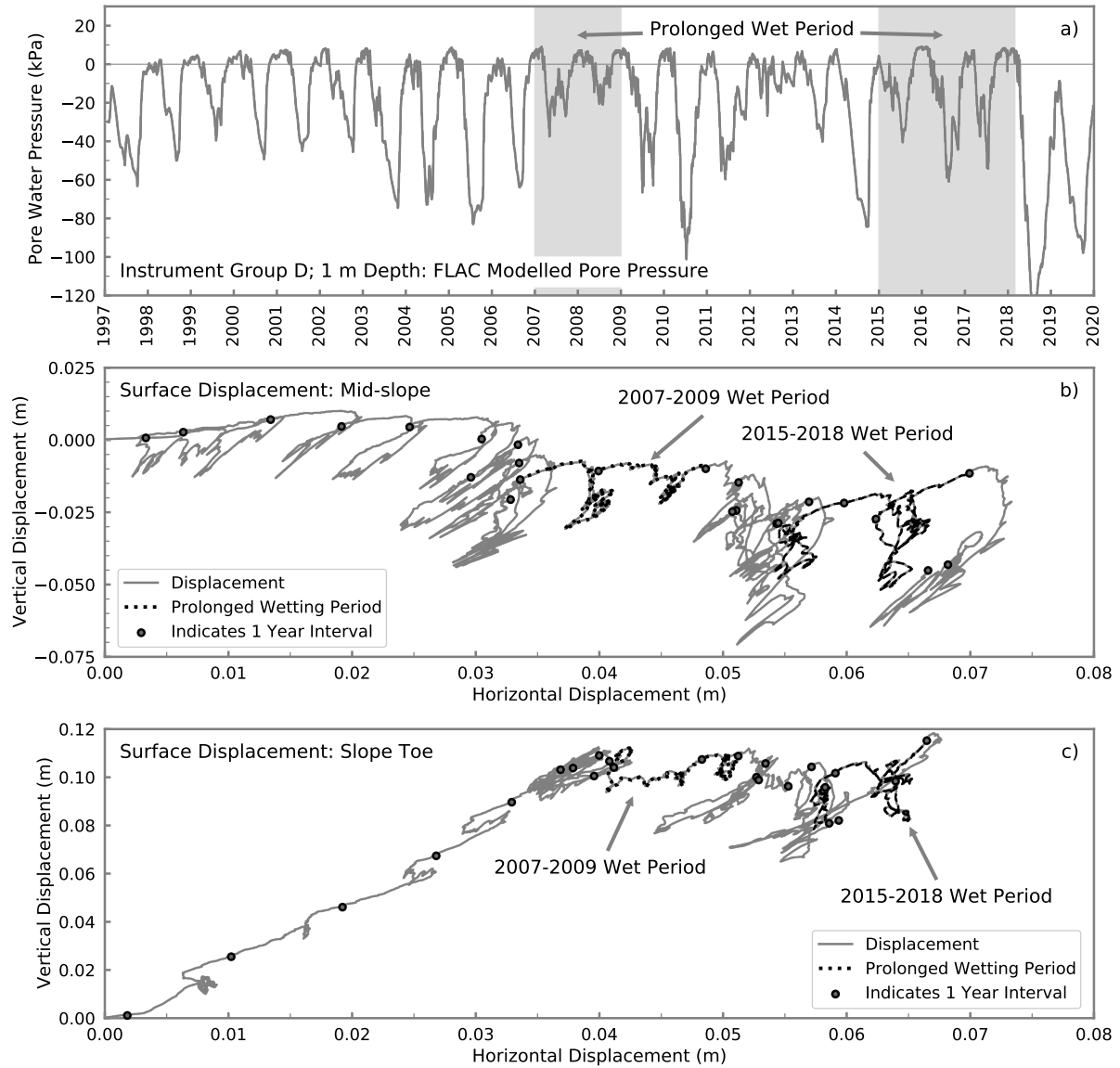
Figure 14: Hydrogeological and mechanical response of Newbury numerical model; a) piezometer D 1.0 m; b) mid-slope displacements; c) toe displacements.

applied to the model grid while maintaining the current in-situ stresses, and material strength properties. The derivation of FoS then commences. This involves an inbuilt FLAC algorithm which applies a trial scaling factor to the shear strength properties; $F_t$; where the trial values of cohesion ($c_t$) and friction angle ($\phi_t$) are derived as follows (see Eqs. (14) and (15):

$$c_t = \frac{1}{F_t} c' \tag{14}$$

$$\phi_t = \frac{1}{F_t} \phi' \tag{15}$$

This is a form of the strength reduction approach (see for example Griffiths and Lane, 1999). Once the trial values of strength are applied, the model is stepped and average grid point unbalanced forces are monitored. If the model returns to equilibrium (a value of average unbalanced force throughout the model is achieved which is lower than a prescribed criterion) this is assumed to represent an upper bound on the current FoS. If however after a prescribed number

of steps, the model equilibrium has failed to converge to the equilibrium value (or converged, but to a value exceeding the criterion) this is assumed to represent a lower bound / unstable FoS. These initial trial upper and lower bound values are then used to define new upper and lower bound $F_t$ values. This process is repeated until the difference between the lower and upper bound $F_t$ values drops below 0.005 giving the FoS at this point in model time. Once this is completed the current FoS is exported and the temporary save file prior to FoS analysis is restored and coupled cycling is continued. As such, the recorded FoS represents a series of discrete records of the slope stability at individual points in time. Full details of the approach are given in (Itasca, 2016).

The results of pore water pressure cycles, displacements, FoS against time and the relative contribution of pore pressure change and strain softening to deterioration are plotted in Fig. 15. Representative critical shear surfaces predicted by the FoS strength reduction calculation at different times for the analysis are presented in Fig. 16.
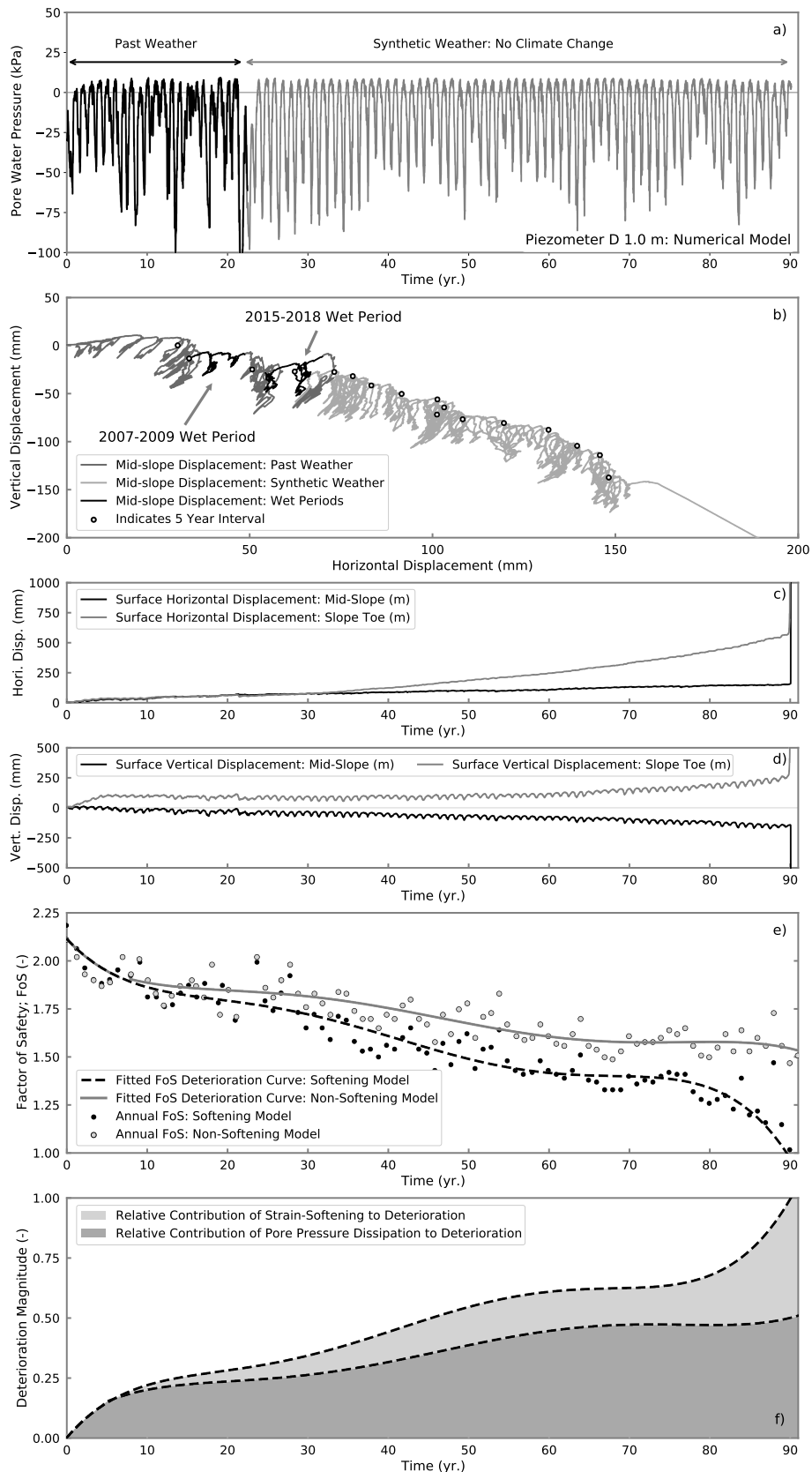
Figure 15: Long-term hydrogeological and mechanical response of Newbury numerical model; a) piezometer B 1.0 m; b) mid-slope displacements; c) toe and mid-slope horizontal displacements; d) toe and mid-slope vertical displacements; e) factor of safety factor of safety analysis; f) contribution of pore pressure dissipation and strain softening to deterioration.
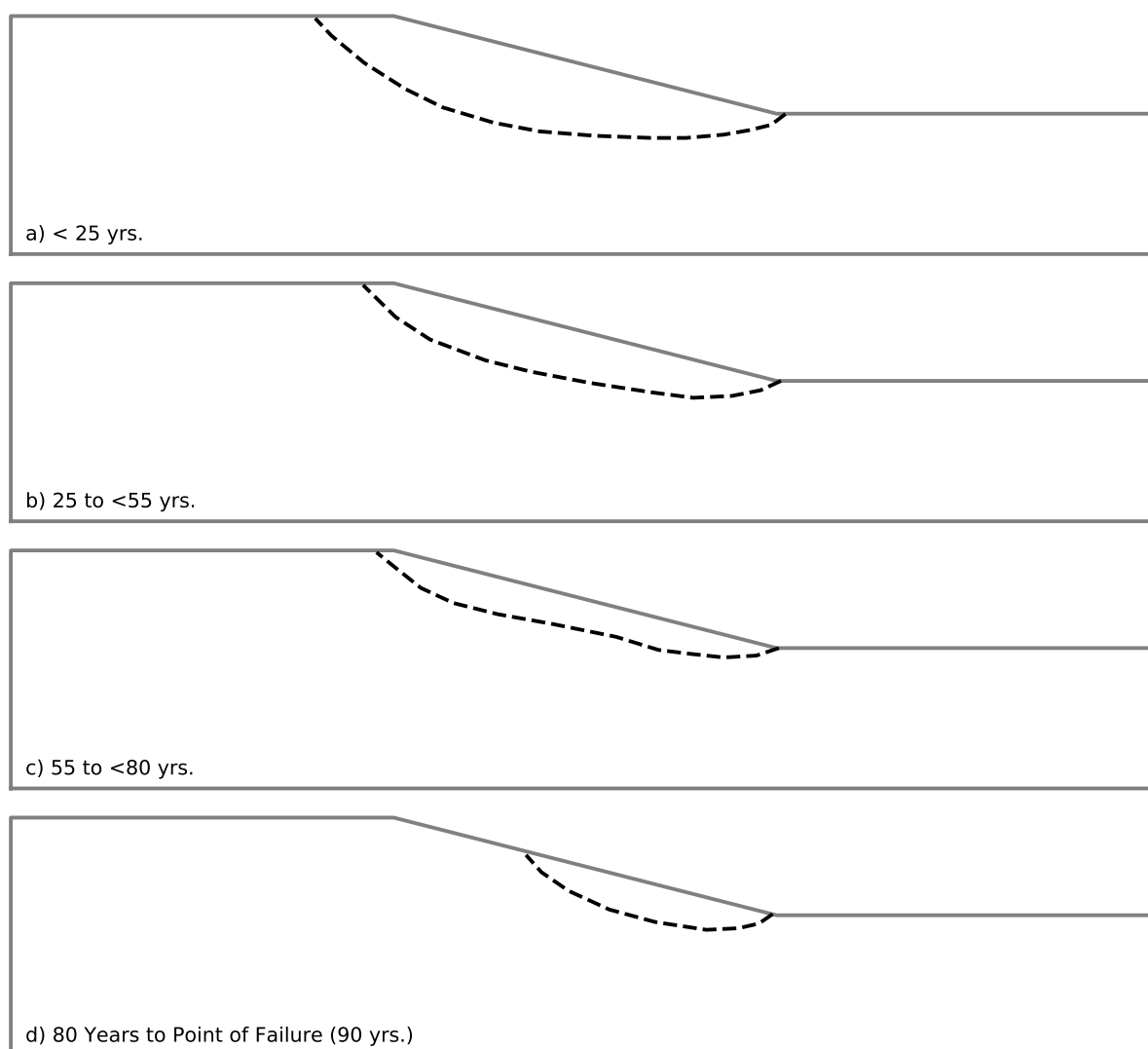
Figure 16: Typical critical failure surfaces for: a) <25 years; b) 25 to <55 years; c) 55 to <80 years and d) 80 years to point of failure.

The seasonal pore water pressure cycles near the toe of the slope during the life of the Newbury cutting slope model are plotted in Fig. 15a, with Fig. 15b illustrating the mid-slope horizontal vs vertical displacements and resultant seasonal shrink/swell cycles. Initially, the slope swells (indicated by net upward and outward displacements). This is indicative behaviour expected due to stress relief and dissipation of post-excavation excess pore water pressures (Vaughan and Walbancke, 1973). The swelling predicted occurs over a period of approximately 15 to 20 years corresponding to the time taken for excess pore water pressure dissipation at shallow depth (i.e. 2.5 m) below the toe of the slope in the numerical analysis. At greater depth (5 m to 10 m) this increases significantly (40 to 50 years) and is consistent with the findings of Vaughan and Walbancke (1973) for similar excavations in low hydraulic conductivity materials such as London Clay.

The 5-year intervals displayed on Fig. 15b demonstrate that after approximately 10 to 15 years, seasonal ratcheting is observed, with gradual outwards and downwards movements with each seasonal cycle of pore water pressure before a sudden failure. The movements predicted are indicative of the mechanism demonstrated by Take and Bolton (2011) experimentally and modelled previously by Postill et al., 2020. The abrupt nature of the failure is emphasised in Fig. 15c

and d which show the horizontal and vertical displacements at the toe and mid-slope which undergo gradual changes until the sudden increase in displacements during year 90 which (along with the FoS dropping below 1) is an indicator of failure. The horizontal displacement at the toe of the slope seems to be a visible early marker of deterioration as this starts to increase in magnitude at approximately 35 years and can be correlated to an increase in average pore water pressure in the toe at 5 and 10 m depth (see Fig. 13b and c). Ultimately the horizontal displacements continue this gradual increase until failure occurs.

Fig. 15e shows the worst case annual FoS values for both the softening model and the control non-softening model. Best fit lines are used to define the resultant deterioration curves. It can be clearly seen that slope deterioration occurs to a lesser extent in the non-softening model and that failure does not occur during the modelled time period. As there is no strain-softening, the resultant reduction in FoS must be purely a result of effective stress changes due to dissipation of construction induced negative pore water pressures. Conversely, the additional reduction in FoS for the softening model must then be attributable to the additional reduction in strength caused by strain-softening. This assumption is used to compare the proportion of total deterioration that can be attributed to pore water pressure dissipation (derived from the non-softening deterioration curve) with that which can be attributed to the strain softening behaviour (the difference between the total deterioration in the softening model and the non-softening model). See Fig. 15f. This shows that the initial rapid dissipation of pore pressure is largely responsible for the initial decrease in FoS during the first 10 years following excavation which is also reflected in Fig. 15e where the FoS for the non-softening and softening models is identical. From this point, the relative importance of strain softening begins to progressively increase over time.

Fig. 17 shows the relationship between average annual pore pressure and displacement increment for the slope toe and mid-slope of the strain softening model. This plot indicates how the average pore pressures tend to become less negative over time with the maximum average negative pore pressures changing from −30 kPa to −20 kPa after 30 to 40 years (see Fig. 17a-d). This corresponds to a gradual increase in horizontal displacement at the toe (see Fig. 15c and Fig. 17) and the increasing divergence between the strain softening and perfectly plastic deterioration curves (Fig. 15e) indicating the increasing importance of permanent strength reduction due to plastic shear strains. From 30 years post excavation to the end of modelling (91 years), the average annual pore pressures appear to stop changing significantly, remaining between −20 kPa and 0 kPa. However, the magnitude of annual toe displacements continues to increase which is indicative of a loss of strength. This trend continues until failure with the largest displacements being seen in Fig. 17g and h which corresponds to the onset of failure from 70 years onwards where the relative contribution of strain softening to deterioration becomes much more important (see Fig. 15e and f) indicating a permanent rather than transient deterioration in factor of safety.
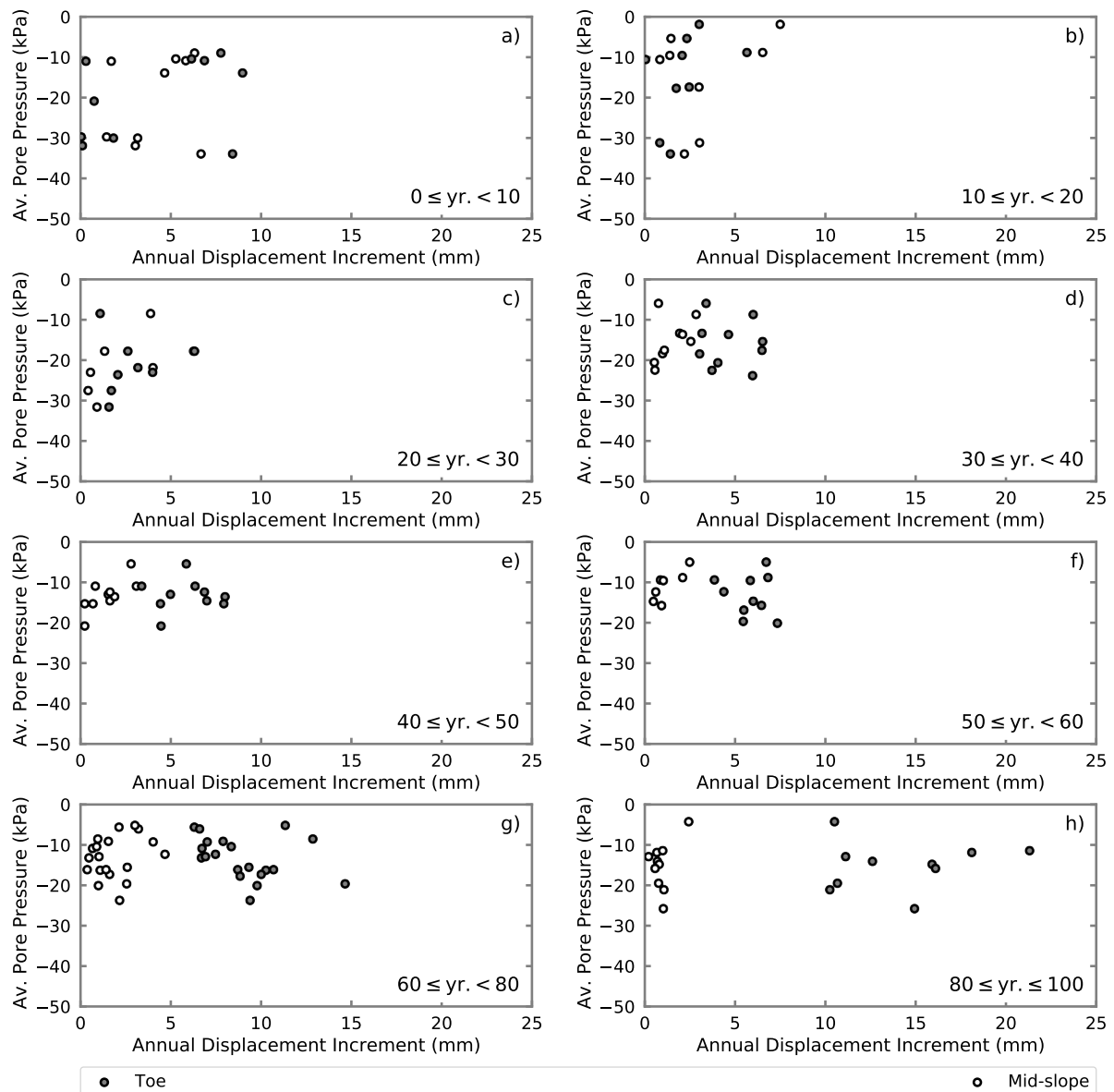
Figure 17: Relationship between average annual pore water pressures at D 1.0 m against toe and mid-slope annual displacements in the strain-softening model for different time periods; a) 0 to <10 years; b) 10 to <20 years; c) 20 to <30 years; d) 30 to <40 years; e) 40 to <50 years; f) 50 to <60 years; g) 60 to <80 years; h) 80 to ≤100 years.

The change in deterioration rate apparent in Fig. 15e corresponds to a change in the dominant failure mechanism from deep to shallow as shown in Fig. 16.

The occurrence of ultimate limit state failure is classified based on a number of criteria, including a reduction in FoS ≤ 1 (see Fig. 15e), a large increase in displacement magnitude (see Fig. 15b, c & d), and a coherently oriented non-zero velocity vector field indicating movement. This in turn corresponds with a region undergoing current plasticity in the model (see. Fig. 18a & b).
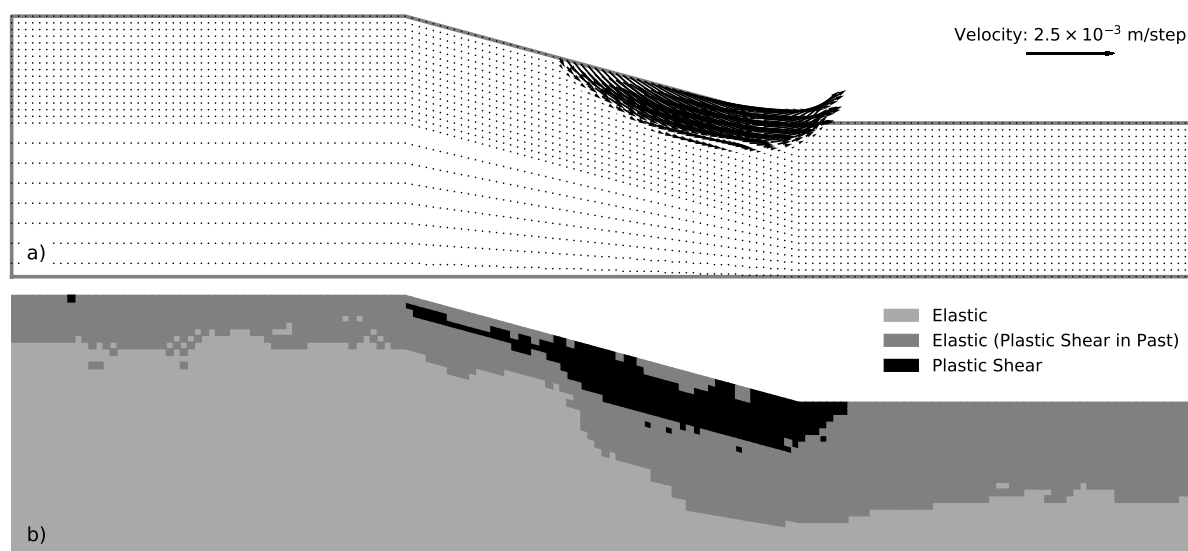
Figure 18: Failure mechanism and criteria; a) velocity vectors showing active failure mechanism with markers for zones undergoing plastic shear strain; b) plastic state indicators showing plastic shear failure corresponding to the movements indicated in a).

When examining Fig. 18a it can be seen that the dominant mechanism starts at the toe and primarily effects the lower half of the slope. Fig. 18b indicates that this mechanism corresponds to a 3 to 4 m thick region currently undergoing plastic shear failure, however it can also be seen that a thinner (1 m thick) band of failed zones extends the full height of the slope to the crest. It is likely that if stepping was allowed to continue, this material would begin to move and due to the shedding of load and loss of support from the failed region, accelerate creating a larger failed mass than that seen initially.

# 6   Discussion

An approach has been presented for modelling long-term deterioration of high-plasticity clay cut slopes with seasonal stress cycles driven by daily boundary conditions.

Hydrogeological behaviour of the numerical analysis has been validated against transient pore water pressure cycles measured in the field over a 16-year period. Mechanical behaviour has also been investigated although it has not been possible to validate this against field data so instead laboratory tests have been replicated. Furthermore, the ability of the slope modelling approach adopted here to replicate displacements driven by surface water flux boundary conditions has been previously validated against centrifuge data in Postill et al. (2020). The time frame over which deterioration of cut slopes occurs, due to post-excavation pore water pressure dissipation and seasonal cycling-driven strain softening, is such that a decadal period of validation is required to give confidence in the model results. While there are other relatively long-term pore pressure monitoring datasets in the literature (See Urciuoli et al., 2016 for an example of a 12 year monitoring period), this comparison of modelled and monitored pore water pressure records over a 16-year period is unique.

Seasonal pore water pressure driven stress cycles are controlled predominantly by the near-surface hydraulic conductivity and the surface-atmosphere interaction, whereas the long-term dissipation of the construction induced pore water pressures is dominated by the deeper, lower

hydraulic conductivity material, as shown by Vaughan and Walbancke (1973). These distinct pore water pressure changes are shown to interact, whereby there is superposition of the short timescale near-surface changes onto the pore water pressure response at depth. This causes suppression of the rate of pore water pressure recovery during drying periods and an acceleration during wet periods. The wetting periods correlate with an increase in the magnitude of annual displacements due to the transient reduction in effective stress and hence shear strength (see for example Lade, 2010). This in turn leads to plastic strain development and depending on the magnitude of this strain, causes softening to occur. Therefore, while the decrease in FoS due to wet periods may be transient due to effective stress change, this in turn can cause permanent reductions in shear strength and hence FoS due to softening (Take and Bolton, 2011; Postill et al., 2020; Rouainia et al., 2020). This critical long-term behaviour has been captured within the presented modelling approach.

The model results demonstrate a change in potential failure mechanism through the life of the slope, whereby the initial critical failure surface is deep seated and rotational, with the primary deterioration being caused by stress relief and post-excavation pore water pressure recovery. With increasing numbers of seasonal cycles, stability of the near-surface zone, which experiences the largest annual stress cycles, begins to deteriorate due to softening and there is a shift in the critical failure to a shallower translational type mechanism (Figs. 15, 16).

The field evidence from Newbury cutting indicates that a zone of elevated near-surface saturated hydraulic conductivity developed rapidly after construction (within 20 years) along the full length of the slope (Dixon et al., 2019). This hydrological deterioration has a significant impact on the surface water balance and pore water pressure cycling within the slope. In order to replicate this observation, the modelling included an elevated saturated hydraulic conductivity and adjustments to the soil water retention properties of the material in this weathered zone. This allowed the numerical model to replicate measured pore water pressure cycles in the near-surface zone with good accuracy. However, this was included in the model immediately after construction, whereas in practice this weathered near-surface zone would develop over time due to vegetation growth and cycles of wetting and drying. The hydrological parameters will change concurrently with mechanical parameters (Stirling et al., 2017, 2020). In future work, improvement of the numerical modelling approach may be possible by employing a constitutive model that is able to replicate this behaviour and more fully capture the coupled mechanical and hydrological aspects of the near-surface weathering process. At present, such a model does not exist.

The modelling also demonstrates the importance of prolonged "wet" periods, defined as a period of limited summer suctions that are dissipated entirely during a subsequent wet winter. This combination leads to elevated pore water pressures for a significant proportion of the year. The magnitude and duration of the associated effective stress cycles cause a change in the mechanical behaviour of the slope, with increased displacements during both the swelling and ratcheting phases. Larger seasonal displacements in wet periods increase the generation of plastic shear strains, leading to increased strain-softening, redistribution of stresses and progressive failure. This process increases the rate of stability deterioration and hence reduces the long-term performance of the slope.

The average size of annual displacement increments was also shown to increase with time, even though the annual pore water pressure cycle size (see Fig. 15a), and the average annual

pore water pressures (Fig. 17d to h) are very similar once the post-excavation equilibration has completed. This change in annual displacement is primarily a function of strength change rather than changes in amplitude in effective stress cycles. This behaviour along with the difference between the strain-softening and perfectly plastic Mohr-Coulomb models (Fig. 15e and f) indicates that the long-term reduction in FoS (i.e. slope performance) is a result of a permanent deterioration in soil strength due to material softening rather than solely a function of transient changes in pore water pressures. This can be seen in the FoS vs time plot (Fig. 15e), with the FoS reducing equally for both the strain-softening and perfectly plastic models for the first 5 years of the life of the slope, followed by an increase in the rate of deterioration past this age, which is characteristic of progressive failure. However the majority of the deterioration in FoS for 3/4 of the slope's life is due to effective stress changes caused by negative pore pressure dissipation and annual pore pressure cycling along with a small but gradually increasing contribution from strength reduction due to strain-softening. Following on from this period where the behaviour is dominated by pore pressure change, is an increase in the rate of deterioration which occurs once the near surface reduction in strength leads to a change in the critical failure mechanism. When this occurs, the near surface seasonal ratcheting mechanism becomes dominant over deep-seated shear strains due to dissipation of excavation excess pore water pressures. The seasonal ratcheting causes progressive reduction in strength in the near surface ultimately leading to a shallower (3.0 m depth, compared to 7.5 m for the initial critical depth <25 years after excavation) first-time failure within the slope which is of a type often observed in grass-covered clay highway slopes (Briggs et al., 2017).

Field monitoring and modelling work (Smethurst et al., 2015; Tsiampousi et al., 2017) has demonstrated that the type of vegetation present can have a positive impact on the stability of slopes in high plasticity clays (while having a negative impact on their serviceability), and conversely vegetation removal can have a negative impact or even be shown to trigger failure. In this work, the vegetation is assumed to be a grass through the life of the slope. In reality this is a simplifying assumption and it is likely that shrubs and in turn trees will develop over time. As the presence of trees has been shown to contribute to stability, this assumption of grass cover throughout is conservative in terms of overall stability but may have implications for the size of annual pore water pressure cycles and further near surface deterioration.

The modelling approach presented captures the primary factors influencing long-term strength deterioration in cutting slopes formed in high plasticity clays (i.e. strain-softening with large reduction in strength from peak to residual and progressive failure). It has been shown that the near-surface weathered zone on the slope plays a fundamental role in long-term behaviour by influencing the in- and out-flow of water at this boundary. However, it is currently not possible to model weathering processes that lead to near-surface hydrogeological deterioration following excavation of the slope and how this develops over time. In order to further develop understanding of slope deterioration behaviour, new constitutive models are required that allow the progressive development of this near-surface zone to be replicated, including the linked changes in saturated hydraulic conductivity, void ratio, water retention behaviour, stiffness and shear strength (Stirling et al., 2017, 2020). The effect of changing vegetation over time and the impact of mechanical root reinforcement will also influence stability and the development of a combined root hydrological and mechanical model would be a significant advance on current capability.

# 7    Conclusions

The paper details a numerical modelling approach that allows forecast of long-term deterioration in the performance of cut slopes formed in high plasticity clays subject to seasonal weather sequences. The following are the main findings:

- Uniquely, hydrological behaviour of the model has been validated using 16 years of field measurements made at multiple locations in a slope. Daily weather inputs have been used to replicate seasonal cycles of pore water pressures.

- Coupled hydrological-mechanical behaviour using an approach validated previously, has been used to forecast long-term deterioration of slope performance as measured by deformation and factor of safety against ultimate limit state failure. It is shown that a seasonal near-surface ratcheting mechanism leads to development of a shallow softened zone (i.e. with reduced shear strength). Seasonal pore water pressure cycles in the slope are regulated by surface-atmospheric interactions coupled with elevated hydraulic conductivity of the near-surface weathered zone that forms post excavation.

- These cycles of pore water pressure, and hence effective stresses, lead to strain softening, strain accumulation and progressive reduction in soil strength in a zone that propagates from the toe of the slope with number of cycles.

- Prolonged periods of elevated pore water pressures (i.e. during wet winters) leads to increased magnitude of slope displacements.

- Cycling of near surface pore water pressures also reduces the rate of dissipation of excavation generated negative excess pore water pressures at depth during dry periods and increase the dissipation rate in wet periods.

- Over a period of decades, the temporal change in pore water pressure regime in the slope alters the dominant potential failure mechanism from deep seated during the initial response to excavation stress changes to a shallow mechanism driven by weather slope surface interactions.

- Modelling outputs show that long-term reduction in factor of safety against shear failure is a function of permanent deterioration of soil shear strength and not just a direct response to seasonal cycles of pore water pressure. This explains observations that a slope can fail under wet winter conditions even though it has remained stable in the past when subject to the same conditions.

This study advances the numerical modelling capability for analysing long-term behaviour of clay cut slopes. It incorporates the governing soil behaviour in a Bishop's effective stress framework (e.g. strain softening and hydraulic conductivity), and captures observed slope mechanisms and failure conditions. The model can be used as a tool to forecast long-term behaviour that leads to deterioration of slope performance for example due to climate change and the efficacy of engineering interventions in slowing deterioration. However, this study also demonstrates the need to include the development of the near-surface weathered zone, post excavation, so that the governing soil properties evolve in this zone over time. Work by Stirling et al. (2017, 2020) has described and started to quantify the magnitude and rate of material degradation mechanisms that result in these modified soil properties.

# Acknowledgements

# References

Alexander, L., Jones, P.D., 2000. Updated Precipitation Series for the U.K. and Discussion of Recent Extremes. Atmos. Sci. Lett. 1, 142-150. https://doi.org/10.1006/asle.2001.0025

Allen, R.G., Pereira, L.S., Raes, D., Smith, M., 1998. Crop evapotranspiration - Guidelines for computing crop water requirements - FAO Irrigation and drainage paper 56 (No. 56). Rome.

Alonso, E.E., Gens, A., Delahaye, C.H., 2003. Influence of rainfall on the deformation and stability of a slope in overconsolidated clays: a case study. Hydrogeol. J. 11, 174-192. https://doi.org/10.1007/s10040-002-0245-1

Anderson, M.G., Hubbard, M.G., Kneale, P.E., 1982. The influence of shrinkage cracks on pore-water pressures within a clay embankment. Q. J. Eng. Geol. Hydrogeol. 15, 9-14. https://doi.org/10.1144/gsl.qjeg.1982.015.01.03

Apted, J.P., 1977. Effects of weathering on some geotechnical properties of London clay. Imperial College London (University of London).

Bažant, Z.P., Pijaudier-Cabot, G., 1988. Nonlocal Continuum Damage, Localization Instability and Convergence. J. Appl. Mech. 55, 287. https://doi.org/10.1115/1.3173674

Bishop, A.W., 1959. The principle of effective stress. Tek. Ukebl. 106, 859-863.

Bishop, A.W., Green, G.E., Garga, V.K., Andresen, A., Brown, J.D., 1971. A New Ring Shear Apparatus and its Application to the Measurement of Residual Strength. Géotechnique 21, 273-328. https://doi.org/10.1680/geot.1971.21.4.273

Blaney, H.F., Criddle, W.D., 1950. Determining Water Requirements in Irrigated Areas from Climatological and Irrigation Data. USDA Soil Cons. Ser. (No. 96).

Blight, G.E., 2003. The vadose zone soil-water balance and transpiration rates of vegetation. Géotechnique 53, 55-64. https://doi.org/10.1680/geot.2003.53.1.55

Briggs, K.M., Dijkstra, T.A., Glendinning, S., 2019. Evaluating the Deterioration of Geotechnical Infrastructure Assets Using Performance Curves, in: International Conference on Smart Infrastructure and Construction 2019 (ICSIC). ICE Publishing, pp. 429-435. https://doi.org/10.1680/icsic.64669.429

Briggs, K.M., Loveridge, F.A., Glendinning, S., 2017. Failures in transport infrastructure embankments. Eng. Geol. 219, 107-117. https://doi.org/10.1016/j.enggeo.2016.07.016

Briggs, K.M., Smethurst, J.A., Powrie, W., O'Brien, A.S., 2013. Wet winter pore pressures in railway embankments. Proc. Inst. Civ. Eng. - Geotech. Eng. 166, 451-465. https://doi.org/10.1680/geng.11.00106

Bromhead, E.N., 1978. Large landslides in London Clay at Herne Bay, Kent. Q. J. Eng. Geol. Hydrogeol. 11, 291-304. https://doi.org/10.1144/GSL.QJEG.1978.011.04.03

Bromhead, E.N., Dixon, N., 1986. The field residual strength of London Clay and its correlation with loboratory measurements, especially ring shear tests. Géotechnique 36, 449-452. https://doi.org/10.1680/geot.1986.36.3.449

Calvello, M., Cascini, L., Sorbino, G., 2008. A numerical procedure for predicting rainfall-induced movements of active landslides along pre-existing slip surfaces. Int. J. Numer. Anal. Methods Geomech. 32, 327-351. https://doi.org/10.1002/nag.624

Chandler, R.J., Skempton, A.W., 1974. The design of permanent cutting slopes in stiff fissured clays. Géotechnique 24, 457-466. https://doi.org/10.1680/geot.1974.24.4.457

Cho, S.E., 2016. Stability analysis of unsaturated soil slopes considering water-air flow caused by rainfall infiltration. Eng. Geol. 211, 184-197. https://doi.org/10.1016/j.enggeo.2016.07.008

Clarke, D., Smith, M., El-Askari, K., 1998. New software for crop water requirements and irrigation scheduling. Irrig. Drain. 47, 45-48.

Cohen, D., Lehmann, P., Or, D., 2009. Fiber bundle model for multiscale modeling of hydromechanical triggering of shallow landslides. Water Resour. Res. 45. https://doi.org/10.1029/2009WR007889

Cotecchia, F., Tagarelli, V., Pedone, G., Ruggieri, G., Guglielmi, S., Santaloia, F., 2019. Analysis of climate-driven processes in clayey slopes for early warning system design. Proc. Inst. Civ. Eng. - Geotech. Eng. 172, 465-480. https://doi.org/10.1680/jgeen.18.00217

Croney, D., 1977. The Design and Performance of Road Pavements. Her Majesty's Stationery Office, London.

Davies, O., Rouainia, M., Glendinning, S., Cash, M., Trento, V., 2014. Investigation of a pore pressure driven slope failure using a coupled hydro-mechanical model. Eng. Geol. https://doi.org/10.1016/j.enggeo.2014.05.012

Di Prisco, C., Imposimato, S., 2003. Nonlocal numerical analyses of strain localisation in dense sand. Math. Comput. Model. 37, 497-506. https://doi.org/10.1016/S0895-7177(03)00042-6

Dixon, N., Bromhead, E.N., 1999. Depth-dependent permeability in London Clay measured using standpipe piezometer equilibration data. Géotechnique 49, 651-660. https://doi.org/10.1680/geot.1999.49.5.651

Dixon, N., Crosby, C.J., Stirling, R., Hughes, P.N., Smethurst, J., Briggs, K., Hughes, D., Gunn, D., Hobbs, P., Loveridge, F., Glendinning, S., Dijkstra, T., Hudson, A., 2019. In situ measurements of near-surface hydraulic conductivity in engineered clay slopes. Q. J. Eng. Geol. Hydrogeol. 52, 123-135. https://doi.org/10.1144/qjegh2017-059

Doorenbos, J., Pruitt, W.O., 1977. Guidelines for Predicting Crop Water Requirements. Food and Agricultural Organisation, Rome, No. 24.

Elia, G., Cotecchia, F., Pedone, G., Vaunat, J., Vardon, P.J., Pereira, C., Springman, S.M., Rouainia, M., Van Esch, J., Koda, E., Josifovski, J., Nocilla, A., Askarinejad, A., Stirling, R., Helm, P., Lollino, P., Osinski, P., 2017. Numerical modelling of slope-vegetation-atmosphere interaction: an overview. Q. J. Eng. Geol. Hydrogeol. 50, 249-270. https://doi.org/10.1144/qjegh2016-079

Ellis, E.A., O'Brien, A.S., 2007. Effect of height on delayed collapse of cuttings in stiff clay. Proc. Inst. Civ. Eng. - Geotech. Eng. 160, 73-84. https://doi.org/10.1680/geng.2007.160.2.73

Galavi, V., Schweiger, H.F., 2010. Nonlocal Multilaminate Model for Strain Softening Analysis. Int. J. Geomech. 10, 30-44. https://doi.org/10.1061/(ASCE)1532-3641(2010)10:1(30)

Garga, V.K., 1970. Residual shear strength under large strains and the effect of sample size on the consolidation of fissured clay. PhD Thesis. University of London (Imperial College of Science and Technology).

Griffiths, D.V., Lane, P.A., 1999. Slope stability analysis by finite elements. Géotechnique 49, 387-403. https://doi.org/10.1680/geot.1999.49.3.387

Hight, D.W., Gasparre, A., Nishimura, S., Minh, N.A., Jardine, R.J., Coop, M.R., 2007. Characteristics of the London Clay from the Terminal 5 site at Heathrow Airport. Géotechnique 57, 3-18. https://doi.org/10.1680/geot.2007.57.1.3

Hu, R., Chen, Y.-F., Liu, H.-H., Zhou, C.-B., 2013. A water retention curve and unsaturated hydraulic conductivity model for deformable soils: consideration of the change in pore-size distribution. Géotechnique 63, 1389-1405. https://doi.org/10.1680/geot.12.P.182

Itasca, 2016. Fast Lagrangian Analysis of Continua V. 8.0 - User's Guide, 6th ed. Itasca Consulting Group Inc., Minneapolis.

Jurečič, N., Zdravković, L., Jovičić, V., 2013. Predicting ground movements in London Clay. Proc. Inst. Civ. Eng. - Geotech. Eng. 166, 466-482. https://doi.org/10.1680/geng.11.00079

Khalili, N., Geiser, F., Blight, G.E., 2004. Effective Stress in Unsaturated Soils: Review with New Evidence. Int. J. Geomech. 4, 115-126. https://doi.org/10.1061/(ASCE)1532-3641(2004)4:2(115)

Kovacevic, N., Hight, D.W., Potts, D.M., 2007. Predicting the stand-up time of temporary London Clay slopes at Terminal 5, Heathrow Airport. Géotechnique 57, 63-74. https://doi.org/10.1680/geot.2007.57.1.63

Kovacevic, N., Hight, D.W., Potts, D.M., Carter, I.C., 2013. Finite-element analysis of the failure and reconstruction of the main dam embankment at Abberton Reservoir, Essex, UK. Géotechnique 63, 753-767. https://doi.org/10.1680/geot.12.P.066

Kovacevic, N., Potts, D.M., Vaughan, P.R., 2001. Progressive failure in clay embankments due to seasonal climate change, in: Proceedings of the International Conference on Soil Mechanics and Geotechnical Engineering. A. A. Balkema, Istanbul, Turkey, pp. 2127-2130.

Lade, P.V., 2010. The mechanics of surficial failure in soil slopes. Eng. Geol. 114, 57-64. https://doi.org/10.1016/j.enggeo.2010.04.003

Leroueil, S., 2001. Natural slopes and cuts: movement and failure mechanisms. Géotechnique 51, 197-243. https://doi.org/10.1680/geot.2001.51.3.197

Lupini, J.F., Skinner, A.E., Vaughan, P.R., 1981. The drained residual strength of cohesive soils. Géotechnique 31, 181-213. https://doi.org/10.1680/geot.1981.31.2.181

Nuth, M., Laloui, L., 2008. Effective stress concept in unsaturated soils: Clarification and validation of a unified framework. Int. J. Numer. Anal. Methods Geomech. 32, 771-801. https://doi.org/10.1002/nag.645

Nyambayo, V.P., Potts, D.M., Addenbrooke, T.I., 2004. The influence of permeability on the stability of embankments experiencing seasonal cyclic pore water pressure changes, in: Jardine, R.J., Potts, D.M. and Higgins, K.G. (Ed.), Advances in Geotechnical Engineering: The Skempton Conference. Thomas Telford, London, pp. 898-910.

O'Brien, A.S., Ellis, E.A., Russell, D., 2004. Old Railway Embankment Clay Fill - Laboratory Experiments, Numerical Modelling and Field Behaviour, in: Jardine, R.J., Potts, D.M. and Higgins, K.G. (Ed.), Advances in Geotechnical Engineering: The Skempton Conference. Thomas Telford, London, pp. 911-921.

Oh, S., Lu, N., 2015. Slope stability analysis under unsaturated conditions: Case studies of rainfall-induced failure of cut slopes. Eng. Geol. 184, 96-103. https://doi.org/10.1016/j.enggeo.2014.11.007

Parker, D.E., Legg, T.P., Folland, C.K., 1992. A new daily central England temperature series, 1772-1991. Int. J. Climatol. 12, 317-342. https://doi.org/10.1002/joc.3370120402

Postill, H., Dixon, N., Fowmes, G., El-Hamalawi, A., Take, W.A., 2020. Modelling seasonal ratcheting and progressive failure in clay slopes: a validation. Can. Geotech. J. 57, 1265-1279. https://doi.org/10.1139/cgj-2018-0837

Potts, D.M., Kovacevic, N., Vaughan, P.R., 1997. Delayed collapse of cut slopes in stiff clay. Géotechnique 47, 953-982. https://doi.org/10.1680/geot.1997.47.5.953

Power, C.M., Abbott, S., 2019. Introduction to ground-related risk to transportation infrastructure. Q. J. Eng. Geol. Hydrogeol. 52, 280-285. https://doi.org/10.1144/qjegh2019-016

Rahardjo, H., Li, X.W., Toll, D.G., Leong, E.C., 2001. The effect of antecedent rainfall on slope stability, in: Unsaturated Soil Concepts and their Application in Geotechnical Practice. Springer Netherlands, Dordrecht, pp. 371-399. https://doi.org/10.1007/978-94-015-9775-3_8

Rahardjo, H., Satyanaga, A., Leong, E.-C., 2013. Effects of flux boundary conditions on pore-water pressure distribution in slope. Eng. Geol. 165, 133-142. https://doi.org/10.1016/j.enggeo.2012.03.017

Rail Accident Investigation Branch, 2017. Rail Accident Report: Derailment due to a landslip, and subsequent collision, Watford (No. 11/2017).

Rouainia, M., Davies, O., O'Brien, T., Glendinning, S., 2009. Numerical modelling of climate effects on slope stability. Proc. Inst. Civ. Eng. - Eng. Sustain. 162, 81-89. https://doi.org/10.1680/ensu.2009.162.2.81

Rouainia, M., Helm, P., Davies, O., Glendinning, S., 2020. Deterioration of an infrastructure cutting subjected to climate change. Acta Geotech. 15, 2997-3016. https://doi.org/10.1007/s11440-020-00965-1

Skempton, A.W., 1964. Long-Term Stability of Clay Slopes. Géotechnique 14, 77-102. https://doi.org/10.1680/geot.1964.14.2.77

Smethurst, J.A., Briggs, K.M., Powrie, W., Ridley, A., Butcher, D.J.E., 2015. Mechanical and hydrological impacts of tree removal on a clay fill railway embankment. Géotechnique 65, 869-882. https://doi.org/10.1680/jgeot.14.P.010

Smethurst, J.A., Clarke, D., Powrie, W., 2006. Seasonal changes in pore water pressure in a grass-covered cut slope in London Clay. Géotechnique 56, 523-537. https://doi.org/10.1680/geot.2006.56.8.523

Smethurst, J.A., Clarke, D., Powrie, W., 2012. Factors controlling the seasonal variation in soil water content and pore water pressures within a lightly vegetated clay slope. Géotechnique 62, 429-446. https://doi.org/10.1680/geot.10.P.097

Smith, P.G.C., 2003. Numerical analysis of infiltration into partially saturated slopes. PhD Thesis. Department of Civil and Environmental Engineering. Imperial College, University of London, UK.

Spink, T., 2019. Strategic geotechnical asset management. Q. J. Eng. Geol. Hydrogeol. qjegh2019-014. https://doi.org/10.1144/qjegh2019-014

Stirling, R., Helm, P., Glendinning, S., Asquith, J., Hughes, P., Toll, D., 2017. Deterioration of geotechnical infrastructure: The influence of asset aging through environmental cycling, in: 19th International Conference on Soil Mechanics and Geotechnical Engineering. Seoul, pp. 3199-3202.

Stirling, R.A., Toll, D.G., Glendinning, S., Helm, P.R., Yildiz, A., Hughes, P.N., Asquith, J.D., 2020. Weather-driven deterioration processes affecting the performance of embankment slopes. Géotechnique 1-13. https://doi.org/10.1680/jgeot.19.sip.038

Summersgill, F.C., Kontoe, S., Potts, D.M., 2017a. Critical Assessment of Nonlocal Strain-Softening Methods in Biaxial Compression. Int. J. Geomech. 17, 04017006. https://doi.org/10.1061/(asce)gm.1943-5622.0000852

Summersgill, F.C., Kontoe, S., Potts, D.M., 2017b. On the use of nonlocal regularisation in slope stability problems. Comput. Geotech. 82, 187-200. https://doi.org/10.1016/j.compgeo.2016.10.016

Summersgill, F.C., Kontoe, S., Potts, D.M., 2018. Stabilisation of excavated slopes in strain-softening materials with piles. Géotechnique 68, 1-14. https://doi.org/10.1680/jgeot.17.P.096

Take, W.A., 2003. The influence of seasonal moisture cycles on clay slopes. PhD Thesis. University of Cambridge. https://doi.org/https://doi.org/10.17863/CAM.19045

Take, W.A., Bolton, M.D., 2004. Identification of seasonal slope behaviour mechanisms from centrifuge case studies, in: Jardine, R.J., Potts, D.M. and Higgins, K.G. (Ed.), Advances in Geotechnical Engineering: The Skempton Conference. Thomas Telford, London, pp. 992-1004.

Take, W.A., Bolton, M.D., 2011. Seasonal ratcheting and softening in clay slopes, leading to first-time failure. Géotechnique 61, 757-769. https://doi.org/10.1680/geot.9.P.125

Thurlby, R., 2013. Managing the asset time bomb: a system dynamics approach. Proc. Inst. Civ. Eng. - Forensic Eng. 166, 134-142. https://doi.org/10.1680/feng.12.00026

Tsiampousi, A., Zdravkovic, L., Potts, D.M., 2017. Numerical study of the effect of soil-atmosphere interaction on the stability and serviceability of cut slopes in London Clay. Can. Geotech. J. 54, 405-418. https://doi.org/10.1139/cgj-2016-0319

Urciuoli, G., Pirone, M., Comegna, L., Picarelli, L., 2016. Long-term investigations on the pore pressure regime in saturated and unsaturated sloping soils. Eng. Geol. https://doi.org/10.1016/j.enggeo.2016.07.018

van Genuchten, M.T., 1980. A Closed-form Equation for Predicting the Hydraulic Conductivity of Unsaturated Soils. Soil Sci. Soc. Am. J. 44, 892-898. https://doi.org/10.2136/sssaj1980.03615995004400050002x

Vaughan, P.R., 1994. Assumption, prediction and reality in geotechnical engineering. Géotechnique 44, 573-609. https://doi.org/10.1680/geot.1994.44.4.573

Vaughan, P.R., Walbancke, H.J., 1973. Pore pressure changes and the delayed failure of cutting slopes in overconsolidated clay. Géotechnique 23, 531-539. https://doi.org/10.1680/geot.1973.23.4.531

Vermeer, P.A., Brinkgreve, R.B.J., 1994. A new effective non-local strain measure for softening plasticity, in: Chambon, R., Desrues, J., Vardoulakis, I. (Eds.), International Workshop on Localization and Bifurcation Theory for Soils and Rocks. Rotterdam, pp. 89-100.

Wilby, R., Dawson, C., Murphy, C., O'Connor, P., Hawkins, E., 2014. The Statistical Down-Scaling Model - Decision Centric (SDSM-DC): conceptual basis and applications. Clim. Res. 61, 259-276. https://doi.org/10.3354/cr01254

Willett, K.M., Dunn, R.J.H., Thorne, P.W., Bell, S., de Podesta, M., Parker, D.E., Jones, P.D., Williams Jr., C.N., 2014. HadISDH land surface multi-variable humidity and temperature record for climate monitoring. Clim. Past 10, 1983-2006. https://doi.org/10.5194/cp-10-1983-2014

Zhang, J., Huang, H.W., Zhang, L.M., Zhu, H.H., Shi, B., 2014. Probabilistic prediction of rainfall-induced slope failure using a mechanics-based model. Eng. Geol. 168, 129-140. https://doi.org/10.1016/j.enggeo.2013.11.005